Bayesian calibration of a non linear damage model of steel structures with random material property: sensitivity analysis and reliability assessment

Clément Freyssinet, Valentine Rey, Franck Schoefs, Tanguy Moro

Bayesian calibration of a non linear damage model of steel structures with random material property: sensitivity analysis and reliability assessment

Clément FREYSSINET[a,b], Valentine REY[a], Franck SCHOEFS[a], Tanguy MORO[b]

[a] *Nantes Université, École Centrale Nantes, CNRS, GeM, UMR 6183, F-44000 Nantes, France.,*
[b] *Nantes Université, IRT Jules Verne, F-44000 Nantes, France.,*

Abstract

For steel structures exposed to environmental loading, Polycyclic fatigue is one of the main causes of mechanical failure. Since a linear damage accumulation does not take into account the loading history, the formulation of a nonlinear accumulation seems to be a particularly suitable approach for minimizing control and maintenance. A deterministic model that takes into account the loading history is therefore chosen and a strategy is proposed to introduce material randomness by Bayesian calibration of the model parameters from random SN-curves. This model is then applied to the case of a tee joint loaded in fatigue for three different loads with random material parameters. On this example, the linear accumulation of damage underestimates the probability of failure compared to the non linear accumulation.

Keywords: Fatigue, Damage model, Material uncertainty, Sensitivity analysis

1. Introduction

A large number of structures must be monitored and inspected to ensure their reliability. The planning of these inspections has to be optimized from reliability assessment (risk-based inspection) [1, 2]. Too frequent inspections increase monitoring costs, whereas too long intervals between inspections can increase repair costs. In-depth knowledge of these structures and their environment allows to identify their failure modes. Then, the development of numerical tools to estimate and predict the state of the structures can be used to plan inspection and maintenance actions.

Fatigue plays a predominant role in the performance of a large number of steel structures such as aircraft [3, 4], ships [5, 6, 7] or offshore platforms [8, 9]. In addition, these structures are subject to uncertainties in geometry [10, 11], material [12, 13] and loading [14, 15, 16] due to the presence of welded joints and environmental conditions. Reliability theory allows accounting for these uncertainties and there relative effect in structural engineering. The performance function $G(t)$ then describes the failure mode at time t. Thus, the probability of failure is $P_f = \text{Prob}(G(t) \leq 0)$. In the case of fatigue, the performance function is usually expressed as $G(t) = D_C - D(t)$, where D_C is the critical damage and $D(t)$ is the damage at time t.

There are many approaches to estimate damage in a semi-probabilistic framework [17, 9]. One of the most popular (especially in the industrial field) is the Rainflow counting and SN (RSN) approach. It consists in four steps: first, an initial study is performed to estimate the structural stress at the point most likely to fail (hot spot stress) [18]. Second, the signal is processed to identify and characterize the cycles that constitute it. This amounts to identifying the $n(\Delta\sigma_i)$ number of cycles of amplitude $\Delta\sigma_i$ where $i \in [\![1; I]\!]$. The most common method is Rainflow counting [19]. Third, each $\Delta\sigma_i$ value is associated with a number of cycles to failure $N(\Delta\sigma_i)$. This association is based on the SN-curves defined as $N(\Delta\sigma_i) = b{\Delta\sigma_i}^a$, where a and b are the SN parameters according to a quantile. Fourth, according to the Palmgreen-Miner formula [20, 21], the total damage is estimated as the sum of the damages caused by the cycles of amplitude $\Delta\sigma_i$ such as $D = \sum_{i=1}^{I} \frac{n(\Delta\sigma_i)}{N(\Delta\sigma_i)}$. Consideration of the loading hazard is then done by defining $\Delta\sigma_i$ as random while consideration of the material hazard is done by defining b as random. The assumption of linear damage accumulation leads to a very cost-effective RSN

approach. However, it assumes that the loading history (the order of cycles) has no effect on the damage and can therefore lead to large approximation errors. Several formulations have been proposed to overcome this problem [17]. However, since they are all based on empirical studies, their applications remain limited. For this reason, continuous damage approaches that take into account the loading history [22, 23, 24] are considered. In this paper, we select the two-scale damage model [25] which is appropriate for polycyclic fatigue of steel structures. Then, the material parameters of the model are considered as random variables and their distribution is identified by calibration from random SN-curves. To perform this calibration, the method proposed in [26] is considered and improved in two aspects: the choice of supports during initialization is optimized and the identified distributions are conservative. Afterwards, to observe the effects of loading history, the model is applied on the study case of a welded joint for three different loads. Finally, the obtained results are compared with those of the RSN approach to quantify the approximation gaps caused by a linear accumulation of damage. Moreover a time variant sensitivity analysis is proposed to analyze the role of each basic random variable during the probabilistic damage propagation.

In Section 2, the two-scale damage (2SD) model of Lemaitre and Doghri is described. In Section 3, a two-step strategy for identifying the distribution of four random material parameters from SN-curves is proposed. Finally, in Section 4, this new method is applied to a welded joint and the estimated probabilities of failure are compared with those of the RSN approach.

2. Non-linear damage accumulation in a deterministic context

To account for the loading history in the damage calculation, the 2SD model of Lemaitre and Doghri [25] is chosen. Indeed, this model is based on the thermodynamics of irreversible processes and it does not require the counting of cycles. It can be used for a wide range of loadings, including non periodic loading for which global energetical approaches cannot be applied [27] and non proportionnal multiaxial loading for which standard approaches such as critical plane analysis [28] are very expensive. Finally, it is appropriate for the polycyclic fatigue of steels structures considered in this paper. In the following subsections, its principle and equations are introduced in a deterministic formalism and then derived for the case of a

uniaxial tensile mechanical problem.

2.1. Description of the two-scale damage model

To investigate the effects of nonlinear damage accumulation, the 2SD model of Lemaitre and Doghri is considered. Polycyclic fatigue tests on steel [29, 30] show the presence of localized cracks at the microscopic scale. Therefore, in [25], a non linear damage model considering a macroscopic scale and a microscopic scale is developed. At the macroscopic scale, the behavior is linear elastic. At the microscopic scale, assuming that the damage occurs during plasticity, the behavior is elastoplastic damaging. The connection between the two scales is then ensured by a localization relationship where only the macroscopic scale affects the microscopic scale. For simplicity, the Lin-Taylor relationship [31] is considered:

$$\boldsymbol{\varepsilon^{\mu}} = \boldsymbol{\varepsilon} \tag{1}$$

Where $\boldsymbol{\varepsilon} = \boldsymbol{\varepsilon^{e}}$ is the macroscopic elastic strain tensor, $\boldsymbol{\varepsilon^{\mu}} = \boldsymbol{\varepsilon^{\mu e}} + \boldsymbol{\varepsilon^{\mu p}}$ is the microscopic strain tensor with an elastic part $\boldsymbol{\varepsilon^{\mu e}}$ and a plastic part $\boldsymbol{\varepsilon^{\mu p}}$ and $\square^{\mu}$ is the notation for quantities at the microscopic scale. At the macroscopic scale, the Hooke's law reads:

$$\boldsymbol{\sigma} = \left(\frac{E}{1-2\nu} \boldsymbol{P^{H}} + \frac{E}{1+\nu} \boldsymbol{P^{D}} \right) : \boldsymbol{\varepsilon} \tag{2}$$

Where $\boldsymbol{\sigma}$ is the Cauchy stress tensor at the macroscopic scale, $\boldsymbol{P^{H}}$ is the hydrostatic projector, $\boldsymbol{P^{D}}$ is the deviatoric projector, E is the Young modulus, ν is the Poisson's ratio and $\boldsymbol{A} : \boldsymbol{B}$ is the double dot product defined by $A_{ijkl}B_{kl}$. At the microscopic scale, the Hooke's law of a damaging material reads:

$$\boldsymbol{\sigma^{\mu}} = (1 - D^{\mu}) \left(\frac{E}{1-2\nu} \boldsymbol{P^{H}} + \frac{E}{1+\nu} \boldsymbol{P^{D}} \right) : \boldsymbol{\varepsilon^{\mu e}} \tag{3}$$

Where $\boldsymbol{\sigma^{\mu}}$ is the Cauchy stress tensor at the microscopic scale and D^{μ} is the damage. To simplify this expression, the effective stress is introduced $\tilde{\boldsymbol{\sigma}}^{\boldsymbol{\mu}} = \frac{\boldsymbol{\sigma^{\mu}}}{(1-D^{\mu})}$:

$$\tilde{\boldsymbol{\sigma}}^{\boldsymbol{\mu}} = \left(\frac{E}{1-2\nu} \boldsymbol{P^{H}} + \frac{E}{1+\nu} \boldsymbol{P^{D}} \right) : \boldsymbol{\varepsilon^{\mu e}} \tag{4}$$

To account for plasticity, a Von Mises yield surface f with linear kinematic hardening $\boldsymbol{X^\mu}$ is used:

$$f = \sqrt{\frac{3}{2}} \| \boldsymbol{P^D} : \tilde{\boldsymbol{\sigma}}^{\boldsymbol{\mu}} - \boldsymbol{X^\mu} \| - \sigma_y^\mu \tag{5}$$

Where $\|\square\|$ stands for the L_2 norm as $\|\boldsymbol{x}\| = \sqrt{\sum_{i,j} x_{ij}^2}$ and σ_y^μ is the yield strength. The hardening evolution is given by:

$$\boldsymbol{dX^\mu} = \frac{2}{3} C(1 - D^\mu) \boldsymbol{d\varepsilon^{\mu p}} \tag{6}$$

Where C is the hardening modulus. The increment of plasticity is defined by:

$$dp^\mu = \sqrt{\frac{2}{3}} ||\boldsymbol{d\varepsilon^{\mu p}}|| \tag{7}$$

In addition, the model predicts a plasticity threshold p_D. When $p^\mu \geq p_D$ the damage is initiated. This damage increment can then evolve as follows:

$$dD^\mu = \left(\frac{Y^\mu}{S} \right)^s dp^\mu \tag{8}$$

Where the elastic energy release rate is $Y^\mu = \frac{1}{2} \tilde{\boldsymbol{\sigma}}^{\boldsymbol{\mu}} : \boldsymbol{\varepsilon^{\mu e}}$ and the damage parameters are S and s. Finally, the critical damage D_C is defined such as $D^\mu \in [0, D_C]$. The case $D^\mu = D_C$ represents the coalescence of microscopic cracks into a macroscopic crack. We consider that rupture occurs only a few cycles after $D^\mu = D_C$. As a consequence, we do not model nor compute the propagation of the macroscopic crack. This assumption is suitable for structures with low redundancy [26].

2.2. Model formulation in the context of a tensile fatigue problem

A calibration of the material parameters from random SN-curves is performed in Section 3. Knowing that most SN-curves are obtained from tension-compression tests with a constant stress amplitude centered at zero, the model is applied in this framework. Considering the equations in Section 2.1 and in the case of a one-dimensional (1D) problem, the following

formula is obtained:

$$\hat{N} = \frac{2C+3E}{6(\Delta\sigma_i - 2\sigma_y^\mu)} p_D + \frac{C(2ES)^s(2s+1)}{3\left(\tilde{\sigma}_i^{\mu\,2s+1} - (2\sigma_y^\mu - \tilde{\sigma}_i^\mu)^{2s+1}\right)} D_C \tag{9}$$

where $\hat{N}$ is the estimated number of cycles to failure ($D^\mu = D_C$), $\Delta\sigma_i$ is the imposed stress amplitude at the macroscopic scale and $\tilde{\sigma}_i^\mu = \frac{C\Delta\sigma_i + 3E\sigma_y^\mu}{2C+3E}$ is the imposed effective stress at the microscopic scale. The proof of this formulation is given in Appendix A.

3. Material parameters calibration from SN-curves in a stochastic context

This section details the calibration of the eight material parameters of the 2SD model from random SN-curves [18]. The SN-curves of a tubular joint are considered here. Since these curves are probabilistic, the calibration consists in identifying the distribution of the material parameters: E, ν, s, σ_y^μ, C, S, p_D, D_C from the distribution of SN-curves. According to the literature [32], for steel studies the coefficients of variation of E and ν are smaller than 5%. Thus E and ν are considered deterministic where $E = 2.1\times10^{11}$ Pa and $\nu = 0.30$. According to Lemaitre, the most appropriate value for the parameter s is 1 [33, 26]. Moreover, the yield strength σ_y^μ is easily identified from SN-curves since it corresponds to the amplitude at which the fatigue limit is reached, i.e. $\sigma_y^\mu = 41.703$ MPa for the SN-curves used in this paper (Figure 1). For these reasons, the parameters $(E, \nu, s, \sigma_y^\mu)$ are considered deterministic and $\boldsymbol{Z} = (C, S, p_D, D_C)$ random. The following subsections present the random SN-curves and the Bayesian calibration techniques. Finally, a two step strategy is proposed to select the supports of the random variables and to identify their distribution. The aim of these two steps is to avoid high numerical costs while obtaining results with high accuracy.

3.1. Description of random SN-curves

Det Norske Veritas (DNV) [18] provides a set of coefficients to model random SN-curves with a bilinear approximation in log-log coordinates. These coefficients come from pratical fatigue tests and are valid for fixed geometry and material properties. The distribution of N for a stress range $\Delta\sigma_i$ in the case of exposition to sea water with cathodic protection is computed

following equation:

$$\log_{10}(N) = \begin{cases} a\log_{10}(\Delta\sigma_i) + \log_{10}(b) & \text{if } \Delta\sigma_i \geq 2\sigma_y^{\mu} \\ +\infty & \text{otherwise} \end{cases} \tag{10}$$

Where a is deterministic and $\log_{10}(b)$ is defined as the realization of $\log_{10}(B) \sim \mathcal{N}(\mathbb{E}, \mathbb{V})$ (normal distribution of expectation $\mathbb{E}$ and variance $\mathbb{V}$.). Each SN-curve $N(\Delta\sigma_i)$ is obtained for one realization of B. In this probabilistic format, a SN-curve represents the set of stress amplitudes $\Delta\sigma_i$ as function of a quantile of N.

In DNV [18], several classes are defined to represent the variety of welded joints and the exploitation conditions (with or without cathodic protection, within sea water or not...). For example, considering that asymptotic fatigue limit is reached for 10^6 cycles, the class T corresponds to a tubular joint and the class D is used for computation at a hot spot. The value of a and the distribution of $\log_{10}(b)$ are identical for these two classes in the case of exposition to sea water with cathodic protection. In Section 4, the study case is a T-joint for which we do the computation at one hot spot. The deterministic value for the slope is $a = -3$. The recommanded value for the variance $\mathbb{V}$ is 0.2^2 in DNV and 0.275^2 in [34]. In this paper, we choose $\mathbb{V} = 0.27^2$ in order to represent the variability of the material. Finally, instead of giving the expectation $\mathbb{E}$, we give the value of $\log_{10}(b)$ corresponding to the quantile 2.3% ($Q_{2.3}$). This value is $\log_{10}(b) = 11.764$. Knowing that $\log_{10}(B)$ follows a distribution $N(\mathbb{E}, \mathbb{V} = 2.7^2)$, it is possible to deduce SN-curves corresponding to other quantiles as shown in Figure 1 for 5% (Q_5) and 25% (Q_{25}). In this Figure, the distribution of $N(\Delta\sigma_i)$ is plotted for each of the 10 stress amplitudes $\Delta\sigma_i$ from the known analytical distribution given in Equation (10). We also plot in Figure 2 the quantiles for different values of the variance $\mathbb{V}$.

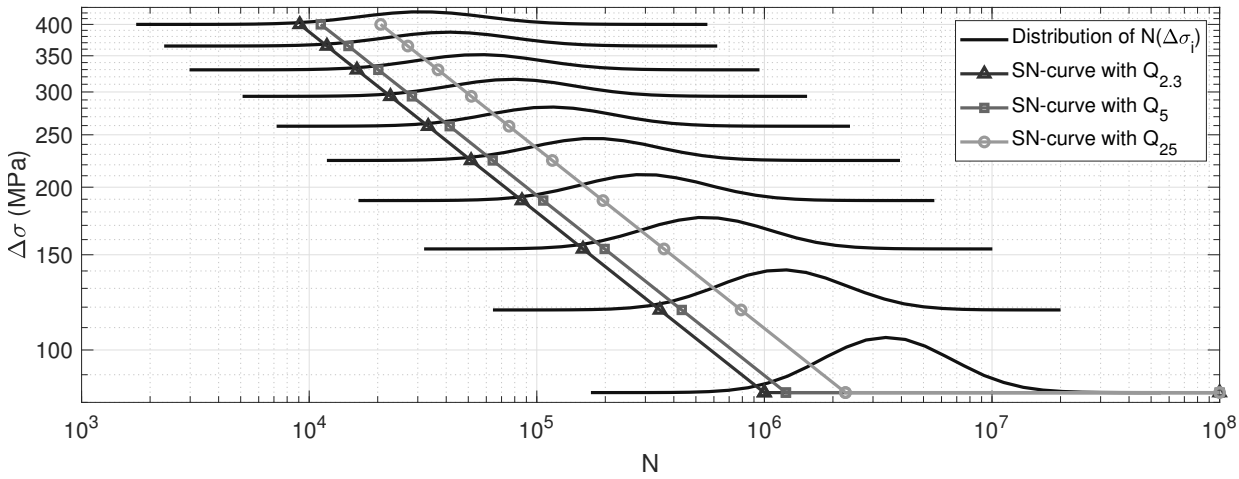

Figure 1: SN-curves for different probabilities of failure

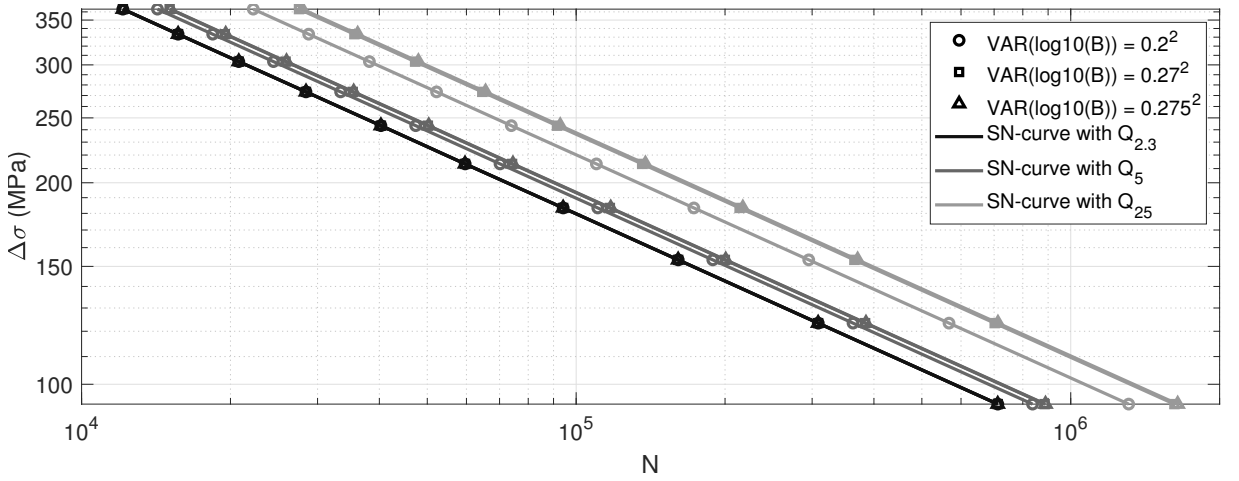

Figure 2: SN-curves for different quantiles and different variances $\mathbb{V}$

3.2. Bayesian Calibration by MCMC

As defined in [35, 36, 37], a Bayesian calibration aims at updating the distribution of one or more random variables $\boldsymbol{Z}$ from a set of observed measurements and a prior knowledge about the distribution. Equation (9) enables to write $\hat{N}$ as a function of $\boldsymbol{Z}$ and $\Delta\sigma_i$. Since there is no parametric distribution as a solution to this problem, $\boldsymbol{Z}$ is estimated by minimizing an error according to a metric and an optimization function. Thus, an error term ξ is expressed such that:

$$N(\Delta\sigma_i) = \hat{N}(\Delta\sigma_i, \boldsymbol{Z}) + \xi \tag{11}$$

It is usually defined as $\xi \sim \mathcal{N}(0, \mathbb{V}_\xi)$ and independent of $\boldsymbol{Z}$ [38]. Since the variance $\mathbb{V}_\xi$ is unknown, it must be estimated. Therefore, it is considered as random and is added to the vector of random variables to be identified $(\boldsymbol{Z}, \mathbb{V}_\xi)$. In this context, Bayes' theorem allows to calculate the posterior distribution $f_{\boldsymbol{Z},\mathbb{V}_\xi}(\boldsymbol{z}, \mathbb{V}_\xi)$ from the prior distribution $p_{\boldsymbol{Z},\mathbb{V}_\xi}(\boldsymbol{z}, \mathbb{V}_\xi)$:

$$f_{\boldsymbol{Z},\mathbb{V}_\xi}(\boldsymbol{z}, \mathbb{V}_\xi) = p_{\boldsymbol{Z},\mathbb{V}_\xi}(\boldsymbol{z}, \mathbb{V}_\xi) L(\boldsymbol{z}, N(\Delta\sigma_i)) c \tag{12}$$

Where $L(\boldsymbol{z}, N(\Delta\sigma_i))$ is the likelihood function of the observations and c is a normalization factor (also called marginal likelihood). Due to the stochastic dimension of the problem, the computation of c is numerically extremely expensive. However, since it is a normalization factor, its value can be neglected in a first step. In a second step, c is computed at a lower cost by normalizing the posterior probability densities. This is the principle of numerous numerical methods such as Variational Bayesian Inference [39], Transport Maps [40] and Monte Carlo Markov Chain (MCMC) [41]. In [26], the authors apply the latter with the Metropolis Hastings algorithm [42, 43]. In presence of very limited previous studies or knowledge, the prior distributions are considered uniform and the likelihood function is defined as follows:

$$\begin{cases} L(\boldsymbol{z}, N(\Delta\sigma_i)) \ = \prod_{i=1}^{I} \varphi_\xi \left(\xi_i\right) \\ \xi_i = \min\limits_{k \in [\![1;K]\!]} |\log_{10}(N_k(\Delta\sigma_i)) - \log_{10}(\hat{N}(\Delta\sigma_i, \boldsymbol{z}))| \end{cases} \tag{13}$$

where I is the number of observed stress amplitudes, K is the number of realizations at each stress amplitude and φ_ξ is the density probability function of ξ. For each stress amplitude $\Delta\sigma_i$, K realizations $N_k(\Delta\sigma_i)$ are obtained using the distribution defined in Equation (10). Note that the SN-curves give the number of cycles to failure $N_k(\Delta\sigma_i)$, while the two-scale damage model (9) gives the number of cycles leading to the formation of a crack at the macroscopic scale $D^\mu = D_C$. Thus, identifying the material parameter distribution of the two-scale damage model using the SN-curves assumes that fatigue damage, when it reaches D_C, leads to failure after few additional cycles.

MCMC calibration methods rely on a key principle: the supports of the distribution should be sufficiently wide to embrace the potential observed realization of each random variable and

sufficiently narrow to avoid high computational costs due to unrealistic realizations. This is challenging for outputs with high variabilities. For this reason, from expert judgment, the authors of [26] had to reduce the size of the supports to a reasonable one before performing the calibration. In the next subsections, this method is improved in two ways: first, by proposing a strategy to justify the choice of supports and second, by adding a conservative criterion during the identification of probabilistic distributions.

3.3. From wide to improved supports

The purpose of this subsection is to select improved supports of prior distributions to avoid high computational costs during the identification of distributions. In [22, 44, 32], several sets of parameters for steel structures are proposed. Using the minimum and maximum values obtained for each of the parameters, supports are provided for each of the random variables $Z_j \in [Z^W_{\min_j}, Z^W_{\max_j}]$ for $j \in [\![1, 4]\!]$ such as:

$$\boldsymbol{Z} = \begin{bmatrix} C \\ S \\ D_C \\ p_D \end{bmatrix} \qquad \boldsymbol{Z^W_{min}} = \begin{bmatrix} 2{\times}10^3 \\ 10^{-3} \\ 0 \\ 0 \end{bmatrix} \begin{matrix} \text{(MPa)} \\ \text{(MPa)} \end{matrix} \qquad \boldsymbol{Z^W_{max}} = \begin{bmatrix} 3{\times}10^6 \\ 7 \\ 1 \\ 10 \end{bmatrix} \begin{matrix} \text{(MPa)} \\ \text{(MPa)} \end{matrix}$$

However, these supports are not consistent for a given material because they mix identification on different type of steels. As a consequence, the objective is to provide improved supports $[Z^*_{\min_j}, Z^*_{\max_j}]$ included in the wide supports $[Z^W_{\min_j}, Z^W_{\max_j}]$ (where W stands for wide). Their boundaries are determined such that the difference between the observed and estimated SN-curves for $Q_{2.3}$ is minimal. This amounts to solving the following problem.

$$\begin{cases} (\boldsymbol{Z^*_{min}}, \boldsymbol{Z^*_{max}}) = \underset{(Z_{\min_j}, Z_{\max_j}) \in \Omega}{\operatorname{argmin}} \left(\left| \frac{a - \hat{a}(\boldsymbol{Z}, \boldsymbol{Z_{min}}, \boldsymbol{Z_{max}})}{a} \right| + \left| \frac{b - \hat{b}(\boldsymbol{Z}, \boldsymbol{Z_{min}}, \boldsymbol{Z_{max}})}{b} \right| \right) \\ \Omega = \{(Z_{\min_j}, Z_{\max_j}) \in [Z^W_{\min_j}, Z^W_{\max_j}] \times [Z^W_{\min_j}, Z^W_{\max_j}] \mid \forall j \in [\![1, 4]\!], Z_{\min_j} < Z_{\max_j}\} \end{cases} \tag{14}$$

Where $(a; \log_{10}(b)) = (-3; 11.764)$ as precised in subsection 3.1 and $(\hat{a}, \hat{b})$ are obtained by linear regression from the 2.3% quantile of $\hat{N}(\Delta\sigma_i, \boldsymbol{Z})$.

Knowing that a and $\log_{10}(b)$ are the slope and y-intercept of the SN-curve, respectively,

One-At-a-Time [45] elastic sensitivity analysis is performed to study the effect of each random variables on $(\hat{a}, \hat{b})$. Figure 3 shows the number of cycles computed with (9) for $I = 10$ and by using three values of Z_j: $Z^W_{\min_j}$, $Z^W_{\max_j}$ and $Z^W_{\text{mean}_j} = \frac{1}{2}(Z^W_{\min_j} + Z^W_{\max_j})$. For each subfigure, the SN-curves with the same markers are obtained by varying the same parameter and fixing the others. Conversely, the SN-curves with the same type of lines are obtained by fixing the same parameter and varying the others. In Figure 3a, for a low value of C, C mainly affects the slope of the SN-curve, while for high value it mainly affects the y-intercept. In Figure 3c, for high values of (C, S, D_C), p_D only affects the slope, while for low values it mainly affects the y-intercept. In Figures 3b and 3d, regardless the values of $(C; p_D)$, S and D_C only affect the y-intercept. As a result, two types of random variables are distinguished: those that affect the y-intercept (C, D_C, S) and those that affect the slope (C, p_D). Based on this observation, the optimization consists in truncating the distributions of $\boldsymbol{Z}$ by reducing the size of its supports. As the truncation on the supports of (C, p_D) affects $\hat{a}$ and as the truncation on the supports (C, D_C, S) affects $\hat{b}$, (14) writes:

$$\begin{cases} (\boldsymbol{Z^*_{\min}}, \boldsymbol{Z^*_{\max}}) = \underset{(Z_{\min_j}, Z_{\max_j}) \in \Omega}{\text{argmin}} \; (\theta + \gamma) \\ \theta = \left| \frac{a - \hat{a}(\boldsymbol{Z}, Z_{\min_1}, Z_{\max_1}, Z_{\min_4}, Z_{\max_4})}{a} \right| \\ \gamma = \left| \frac{b - \hat{b}(\boldsymbol{Z}, Z_{\min_1}, Z_{\max_1}, Z_{\min_2}, Z_{\max_2}, Z_{\min_3}, Z_{\max_3})}{b} \right| \\ \Omega = \{(Z_{\min_j}, Z_{\max_j}) \in [Z^W_{\min_j}, Z^W_{\max_j}] \times [Z^W_{\min_j}, Z^W_{\max_j}] \mid \forall j \in [\![1, 4]\!], Z_{\min_j} < Z_{\max_j}\} \end{cases} \tag{15}$$

Finally, the values of (I, K) must be determined. To achieve a confidence level of 99% in the description of $N(\Delta\sigma_i)$, K is set equal to $2{\times}10^4$. Then, the larger I, the better stresses are discretized and the longer the computation time. A compromise is found with $I = 10$ for $\Delta\sigma \in [93.4, 493.4]$ MPa. For $(I, K) = (10, 2{\times}10^4)$, the optimization is performed by solving (15). The following results are obtained.

$$\begin{cases} C & \in [2{\times}10^6; 3{\times}10^6] \text{ (MPa)} \\ S & \in [10^{-3}; 1] \qquad \text{(MPa)} \\ D_C & \in [0; 0.5] \\ p_D & \in [0; 1] \end{cases} \tag{16}$$

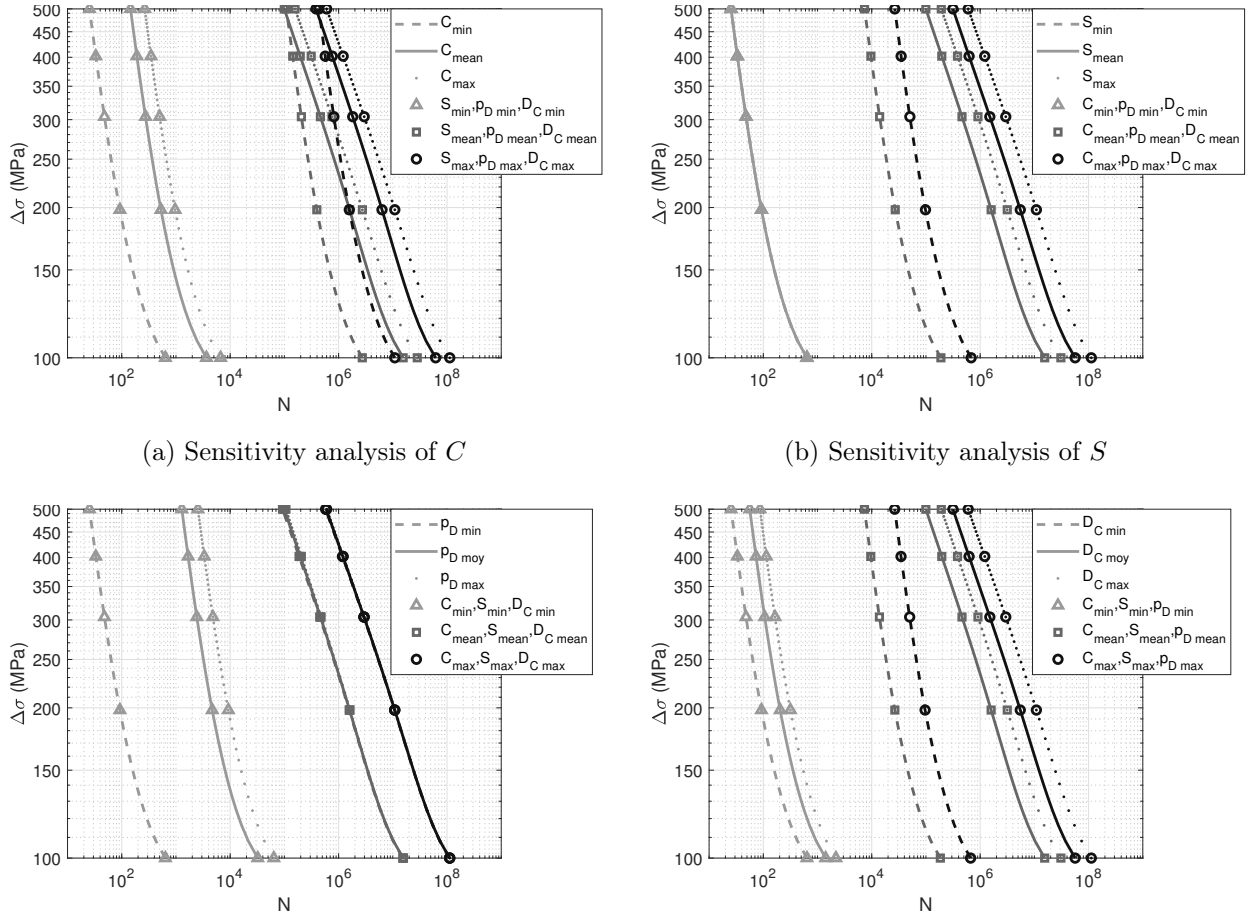

(a) Sensitivity analysis of C

(b) Sensitivity analysis of S

(c) Sensitivity analysis of p_D

(d) Sensitivity analysis of D_C

Figure 3: Elastic sensitivity analysis of $\boldsymbol{Z}$

3.4. Identification of the probabilistic distributions with a conservative criterion

The purpose of this subsection is to improve the identification method proposed in [26] to achieve a better fitting while ensuring conservative SN-curves: the quantile of SN-curves built with 2SD model should be less than the $Q_{2.3}$ of the reference whatever the stress. Since MCMC is not a deterministic method, it is possible to exploit its variability in output. $L \times M$ identifications of $\boldsymbol{Z}$ are performed, where L is the number of resampling observed $2{\times}10^4$ data sets $N_k(\Delta\sigma_i)$ and M is the number of identified distributions by parameters performed for each data set. As a consequence, $L \times M$ estimated SN-curves are built for $Q_{2.3}$. Finally, the most accurate identification of $\boldsymbol{Z}$ is the one that minimizes the error between observed and estimated SN-curves. For $l \in L$, the observations affect the identification of $\boldsymbol{Z}$ and hence $\hat{N}_{l,m}$. The error $\beta_{l,m}$ is the sum over all the stress amplitudes of the relative error between the number of cycles leading to rupture N (see Equation (10)) and the estimated number of cycles leading to

rupture $\hat{N}$ (see Equation (9)). It is written:

$$\beta_{l,m} = \sum_{i=1}^{I} \frac{|b\Delta{\sigma_i}^a - \hat{N}_{l,m}(\Delta\sigma_i, \boldsymbol{Z})|}{b\Delta{\sigma_i}^a} \tag{17}$$

It is also desirable to obtain optimal and conservative set (l^*, m^*) that underestimate the number of cycles to failure. The problem writes:

$$\begin{cases} (l^*, m^*) & = \underset{(l,m)\in U}{\arg\min}\ \beta_{l,m} \\ U & = \{(l,m) \in [\![1;L]\!] \times [\![1;M]\!]\} \cap \{(l,m) \in {\mathbb{N}^*}^2 \mid \forall i \in [\![1;I]\!],\ b\Delta{\sigma_i}^a - \hat{N}_{l,m}(\Delta\sigma_i, \boldsymbol{Z}) \geq 0\} \end{cases} \tag{18}$$

Finally, the values of (L, M) must be determined. MCMC computational time is driven by several factors: the cost of the model, the width of the distribution supports, the shape of the prior distributions, the correlation between the variables and the number of random variables. The model is analytical and the support of the distributions is selected as narrow as possible. Therefore, these two factors reduce numerical costs. However, four random variables are considered, the prior distributions are chosen uniform (which is the less informative distribution) and it is very difficult to assume correlation between the random variables. Therefore, these three factors increase numerical costs and lead to slow convergence: for $(L, M) = (1, 1)$ the average time for an identification of 10^4 realizations is about 45 minutes with around 2.5×10^5 calls to the model. Using the MCMC algorithm, two independent convergence studies are performed. In the first one, $M = 1$ is fixed and L varies on the interval $[\![1; 20]\!]$. In the second one, $L = 1$ is fixed and M varies on the interval $[\![1; 20]\!]$. The maximum computation time is fixed to 3.5 days (5040 minutes),then $L \times M$ must be less than or equal to 112. The problem writes:

$$\begin{cases} (L^*, M^*) & = \underset{(L,M)\in V}{\arg\min}\ \left(\sum_{m=1}^{M} \beta_{1,m} + \sum_{l=1}^{L} \beta_{l,1}\right) \\ V & = \{(L,M) \in [\![1;20]\!] \times [\![1;20]\!]\} \cap \{(L,M) \in {\mathbb{N}^*}^2 \mid L \times M \leq 112\} \end{cases} \tag{19}$$

After the computation of the quantity $\left(\sum_{m=1}^{M} \beta_{1,m} + \sum_{l=1}^{L} \beta_{l,1}\right)$ for all couples $(L, M) \in V$, the optimal couple $(L^*, M^*) = (10, 10)$ is obtained. This optimization is carried out on a grid to

avoid any local minimum solution. The MCMC output variability domain and the optimal SN-curves with and without this conservative criterion are plotted in Figure 4. Each point represents the number of cycles to failure estimated for a given stress amplitude. For each curve, the estimated points are aligned. This property is not imposed during MCMC and confirms the idea that the size of the populations generated by MCMC is large enough (for evaluating a 2.3% quantile) and that the 2SD model suits the properties of an SN-Curve. Figure 4 also shows that the optimal non conservative set overestimates the number of cycles to failure for $\Delta\sigma_i \geq 257.6$ MPa. To thoroughly illustrate the identification, in Figure 5, we give both the $Q_{2.3}$ quantile and the distributions of number of cycles to failure generated from the SN-curve using Equation (10) (observations) and the number of cycles to failure obtained after the Bayesian calibration with the continuous damage model. The relative errors between the estimated and observed number of cycles to failure are listed in Table 1. The signs confirm the previous remark. Note that the errors are very high for $\Delta\sigma_1 = 93.40$MPa. This is justified by the shape of the SN-curves obtained with the 2SD model. Indeed, there curves are of class C^1 unlike the observed SN-curves which are bilinear, as illustrated in Figure 6. Thus, for loads with stress amplitude close to the asymptotic fatigue limit, the two approaches are no longer comparable. However, there is no consequence since the 2SD model is not dedicated to gigacyclic fatigue, but only to polycyclic fatigue.

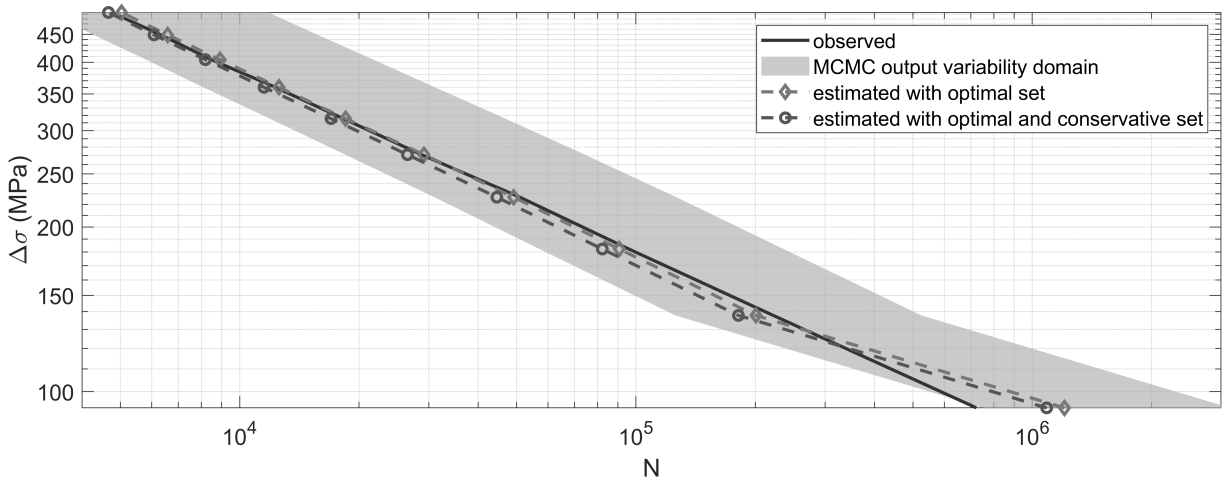

Figure 4: SN-curves with an without conservative criterion

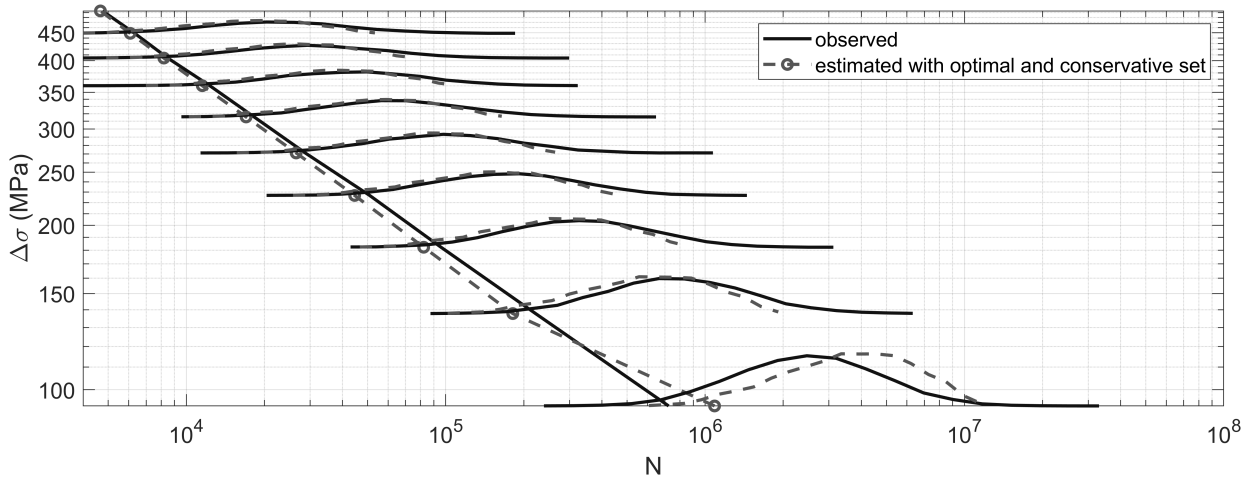

Figure 5: SN-curves (2.3% quantile) and distributions for observations and optimal and conservative set

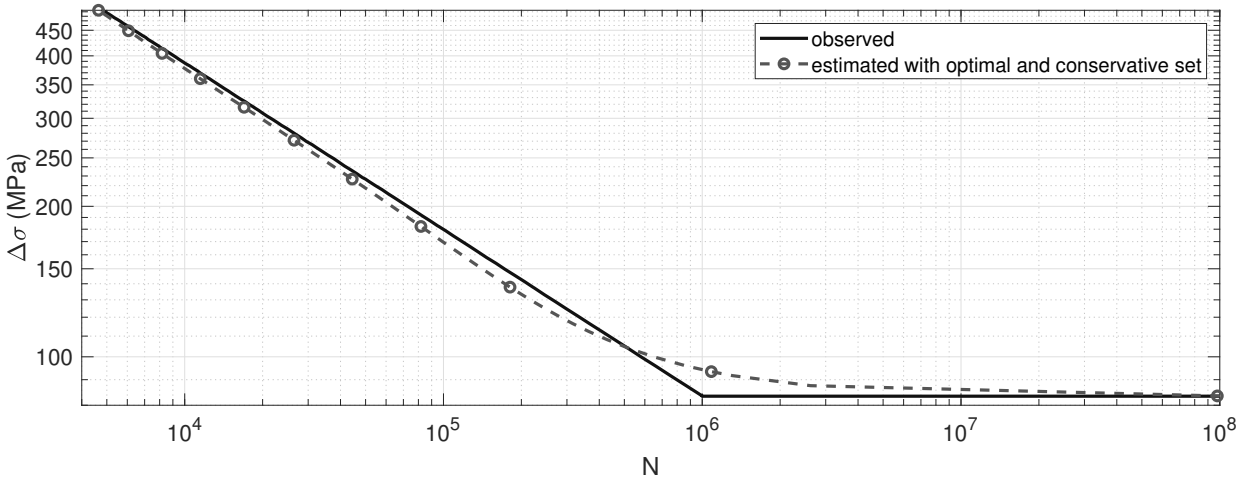

Figure 6: Q2.3 quantile for SN-curve (oberserved) and identified

$\Delta\sigma_i$ (MPa)	Relative error for optimal set	Relative error for optimal and conservative set
93.40	-66.77	-50.34
137.8	9.62	18.33
182.3	5.42	14.29
226.7	3.55	12.50
271.2	-1.46	7.81
315.6	-1.36	6.91
360.1	-2.02	6.46
404.5	-5.09	3.43
449.0	-4.14	3.85
493.4	-5.88	1.86

Table 1: Relative error (%) between estimated and observed number of cycles to failure for $Q_{2.3}\%$

Statistics of $\boldsymbol{Z}$ and their coefficient of variation are given in Tables 2 and 3 for the set (l^*, m^*). The only non-negligible correlation coefficient is $R(S, D_C) = -0.260$ meaning that (S, D_C) are fairly linearly correlated. Since these coefficients provide limited information, they are completed by studying the joint distributions plotted in Figure 7. No significant nonlinear correlation is observed. The random variables C and p_D are therefore considered independent and S and D_C correlated. Moreover, the distributions of C and p_D are close to uniform distributions. Distributions of the parameters being identified, 2SD model and RSN approach are compared in Section 4.

	C (MPa)	S (MPa)	D_C	p_D
Mean	2.507×10^6	0.612	0.303	0.554
Standard deviation	2.900×10^5	0.2313	0.116	0.260

Table 2: Means and standard deviations of $\boldsymbol{Z}$

R	C (MPa)	S (MPa)	D_C	p_D
C (MPa)	1	-0.058	-0.039	0.003
S (MPa)	-0.058	1	-0.260	-0.022
D_C	-0.039	-0.260	1	-0.019
p_D	0.003	-0.022	-0.019	1

Table 3: Bravais-Pearson correlation coefficients of $\boldsymbol{Z}$

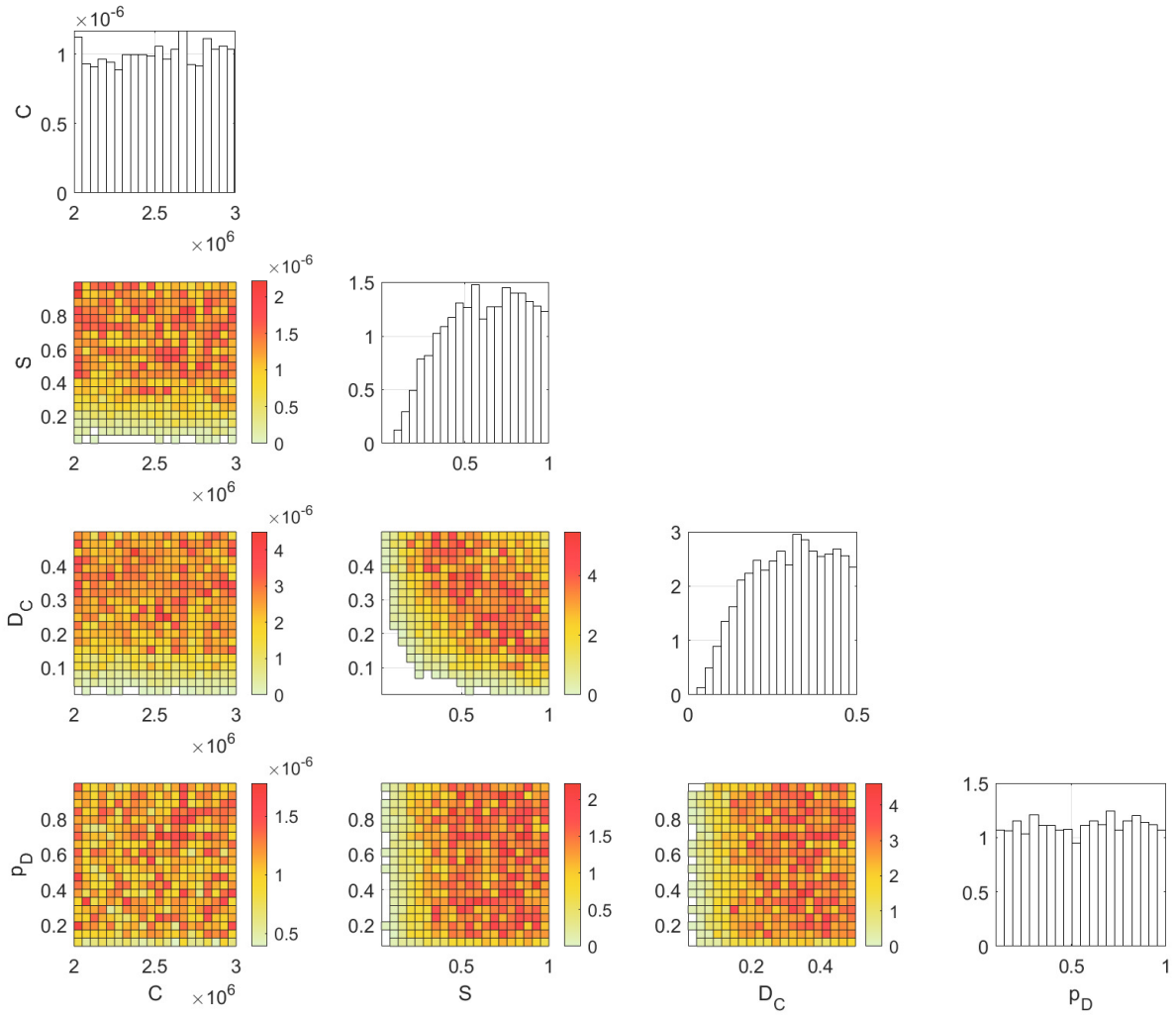

Figure 7: Joint and marginal distributions of $\boldsymbol{Z}$

4. Comparison of damage estimated by linear and non-linear accumulation in a stochastic context

To compare the 2SD model with the RSN approach, the case of a cantilever plate welded to a rigid plate and loaded in bending is considered. It is representative of the loading of steel

bridges, ships and offshore studies. Three loads that result in the same damage according to the RSN approach and represent three time series are then generated. After propagating the material uncertainties, the final damage distribution is analyzed for each load and a sensitivity analysis of the damage with respect to $\boldsymbol{Z}$ is performed. Finally, the three probabilities of failure are estimated and compared with those from the RSN approach.

4.1. Study case: modeling of a welded joint

As illustrated in Figure 8, two rectangular plates P_1 and P_2 in the plane Oxy are considered and welded to form a T-joint. Since this type of structure is most sensitive to bending, a distributed load along y is applied to the boundary of P_2 on the opposite side of the weld. To simplify the study, P_1 is considered infinitely rigid and stress concentrations due to welding are not accounted for. Finally, P_2 is isolated and modeled by a two-dimensions (2D) rectangular structure clamped at $x = 0$ and loaded on the opposite side. For the 2SD model, at the macroscopic scale, the behavior is assumed to be linear elastic isotropic, where $E = 2.1{\times}10^{11}$ Pa and $\nu = 0.30$. At the microscopic scale, the behavior is assumed to be isotropic elastoplastic damaging, where $E = 2.1{\times}10^{11}$ Pa, $\nu = 0.30$, $s = 1$ and $\sigma_y^{\mu} = 41.703$ MPa are the deterministic microscopic parameters and $\boldsymbol{Z} = (C, S, p_D, D_C)$ are the stochastic microscopic parameters whose distributions were identified in subsection 3.4. The structure is meshed with quadrilateral elements and only one element is considered damageable. Since cracks often occur in the neighborhood of the filet weld, the hot spot is located near the clamping. The damageable element is therefore positioned in this area (black finite element in Figure 8).

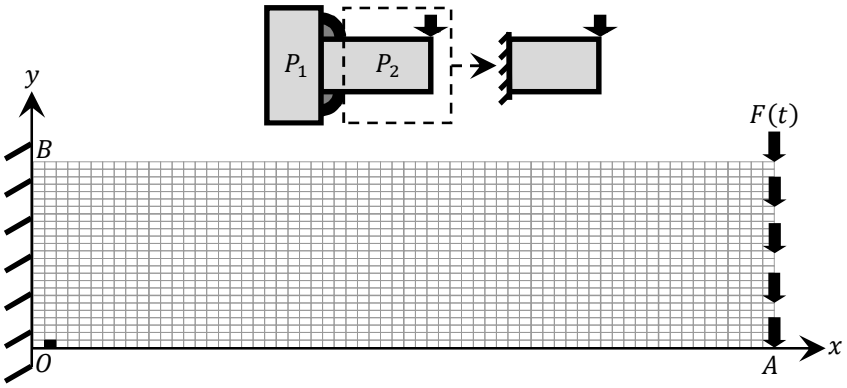

Figure 8: Modeling, boundary conditions and mesh of P_2

The objective of this section is to analyze the effect of the load history by comparing the 2SD model and the RSN approach with random material properties. Three loads $F_q(t)$ for $q \in \{1, 2, 3\}$ with increased complexity are defined according to two criteria:

- Equivalent number of cycles n^*
- Equivalent damage D^* according to the RSN approach

Since the defined problem is driven by an imposed load $F_q(t)$ and the damage calculation is driven by the local stress $\boldsymbol{\sigma_q}(x_0, y_0, t)$ in the damageable element centered in (x_0, y_0), a relationship must be defined between $F_q(t)$ and $\boldsymbol{\sigma_q}(x_0, y_0, t)$. When the 2SD model is applied in 2D, the local stress is written:

$$\boldsymbol{\sigma_q}(x_0, y_0, t) = \begin{bmatrix} \sigma_{xx_q}(x_0, y_0, t) & \sigma_{xy_q}(x_0, y_0, t) \\ \sigma_{xy_q}(x_0, y_0, t) & \sigma_{yy_q}(x_0, y_0, t) \end{bmatrix} \tag{20}$$

Parameters of the 2SD model being identified from a 1D test we first check that we are close to this configuration. According to location of the damageable element and boundary conditions, the damageable element is mainly stressed in tension-compression. The effects of $\sigma_{yy_q}(x_0, y_0, t)$ and $\sigma_{xy_q}(x_0, y_0, t)$ being weak, the von Mises stress (21) will be used for both the RSN and the 2SD model whose parameters are the same in all the direction (isotropy of damage model).

$$\sigma_q(x_0, y_0, t) = \sqrt{\frac{3}{2}} \left\| \boldsymbol{P^D} : \boldsymbol{\sigma}_q(x_0, y_0, t) \right\| \tag{21}$$

Since at the macroscopic scale the behavior is linear elastic, $\sigma_q(x_0, y_0, t)$ is written:

$$\sigma_q(x_0, y_0, t) = \alpha(x_0, y_0) F_q(t) \tag{22}$$

Where $\alpha(x_0, y_0)$ only depends on the geometry. Finally, all that remains is to define $\sigma_q(x_0, y_0, t)$ for $q \in \{1, 2, 3\}$ as function of D^* and n^*. The most simple stress signal $\sigma_1(x_0, y_0, t) = \alpha(x_0, y_0) F_1(t)$ is a sinus with a constant amplitude stress $\Delta\sigma_{1,1}$ and $n(\Delta\sigma_{1,1})$ cycles. To avoid any effect of the mean stress, $\sigma_1(x_0, y_0, t)$ is centered in 0. The associated final damage is then

written $D_1 = \frac{n(\Delta\sigma_{1,1})}{N(\Delta\sigma_{1,1})}$. The period T_1 and the stress amplitude $\Delta\sigma_{1,1}$ are chosen such as:

$$\begin{cases} \frac{n(\Delta\sigma_{1,1})}{N(\Delta\sigma_{1,1})} & = D^* \\ n(\Delta\sigma_{1,1}) & = n^* \end{cases} \tag{23}$$

According to (10) and knowing that the considered time domain is $t \in [t_0; t_{end}]$, the system becomes:

$$\begin{cases} \Delta\sigma_{1,1} & = \left(\frac{n^*}{bD^*}\right)^{\frac{1}{a}} \\ T_1 & = \frac{t_{end}}{n^*} \end{cases} \tag{24}$$

The second signal $\sigma_2(x_0, y_0, t) = \alpha(x_0, y_0)F_2(t)$ is a realization of a Gaussian process with Gaussian correlation. Its parameters are the variance $\mathbb{V}_2$, expected value $\mathbb{E}_2$ and correlation length $\mathbb{L}_2$. As for $\sigma_1(t)$, $\mathbb{E}_2$ is set equal to zero. Knowing that $\mathbb{V}_2$ affects $\Delta\sigma_{i,2}$ while $\mathbb{L}_2$ affects $n(\Delta\sigma_{i,2})$, $\mathbb{L}_2$ is first computed with (25) by setting a variance $\mathbb{V} = 1$ arbitrarily then $\mathbb{V}_2$ is computed with (26).

$$\mathbb{L}_2 = \underset{\mathbb{L}\in\mathbb{R}^+}{\operatorname{argmin}} \left| n^* - \sum_{i=1}^{I} n\left(\Delta\sigma_{i,2}(\mathbb{V}), \mathbb{L}\right) \right| \tag{25}$$

$$\mathbb{V}_2 = \underset{\mathbb{V}\in\mathbb{R}^+}{\operatorname{argmin}} \left| D^* - \sum_{i=1}^{I} \frac{n\left(\Delta\sigma_{i,2}(\mathbb{V}), \mathbb{L}_2\right)}{N(\Delta\sigma_{i,2}(\mathbb{V}))} \right| \tag{26}$$

The last signal, $\sigma_3(x_0, y_0, t) = \alpha_{xx}(x_0, y_0)F_3(t)$ is a realization of a Gaussian process with Matern correlation. It allows the introduction of small irregularities (which could represent measurement uncertainties, for example) compared to $\sigma_2(x_0, y_0, t)$. Its parameters are assumed to be identical to those used for $\sigma_2(x_0, y_0, t)$. The $\sigma_2(x_0, y_0, t)$ and $\sigma_3(x_0, y_0, t)$ realizations of the random field were generated using the Uqlab framework [46] through Karhunen Loève expansion [47]. With $(n^*, D^*) = (10^4, 1)$ and $(t_0, t_{end}) = (0; 1.06\times10^4)$, the parameters obtained for each signal are the following:

- For $\sigma_1(t)$, $\Delta\sigma_{1,1} = 385$ MPa and $T_1 = 1.04$
- For $\sigma_2(t)$, $\mathbb{V}_2 = 2.59\times10^4$ MPa^2 and $\mathbb{L}_2 = 0.30$

- For $\sigma_3(t)$, $\mathbb{V}_3 = 2.59{\times}10^4$ MPa^2 and $\mathbb{L}_3 = 0.30$

Finally, truncated series of the signals are shown in Figure 9 where $t \in [4958.6; 4969.5]$. An example with two signals composed of two amplitudes of sinus is developed in Appendix B to illustrate the ability of the 2SD model to take into account the loading history.

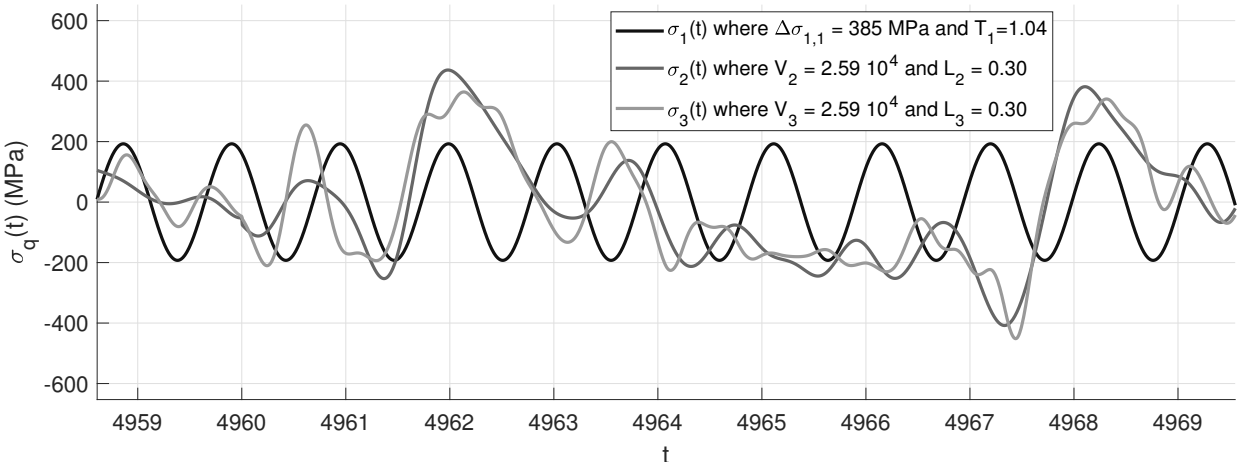

Figure 9: Truncated series of the three signals where $t \in [4958.6; 4969.5] \subset [t_0; t_{end}]$

4.2. Propagation of material uncertainty

Two strategies to compute the fatigue damage are compared: the RSN approach and the 2SD model. To propagate the material uncertainty, a sample P of 5000 realizations is considered. It is sufficient for evaluating a 2.3% quantile.

4.2.1. Propagation of material uncertainty with the Rainflow counting and SN approach

In the case of the RSN approach, the material uncertainty comes from the random variable B in (10). A population of P realizations of B are randomly generated by latin hypercube sampling and for each of them, the final damage is calculated such as:

$$D(t_{end}) = \sum_{i=1}^{I} \frac{n(\Delta\sigma_i)}{b{\Delta\sigma_i}^a} \tag{27}$$

Figure 10 plots the final damage distributions $D(t_{end})$. Regardless of the applied stress, the distribution of the final damage is equivalent to a lognormal distribution. Moreover, the damage distributions do not have a finite upper bound. This is a consequence of the damage formulation,

which does not take into account the critical damage. Finally and as expected, the final damage distributions are equivalent for the first two loadings.

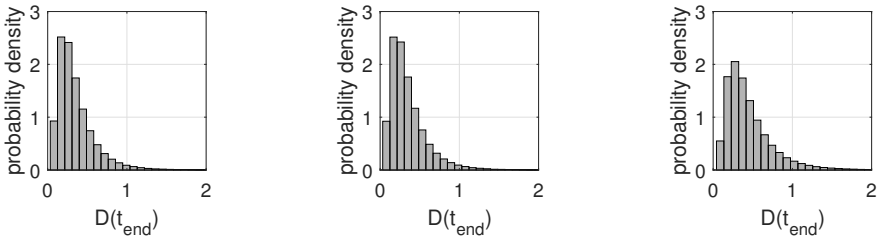

(a) First loading (b) Second loading (c) Third loading

Figure 10: Probability densities of $D^{\mu}(t_{end})$ computed with the RSN approach

4.2.2. Propagation of material uncertainty with the two-scale damage model

Equations (1) to (8) are discretized with a time step $\Delta t = 0.005$ and a radial return algorithm is used. A sample of P realizations of $\boldsymbol{Z}$ is then randomly generated by latin hypercube sampling and rejection sampling (to preserve the correlation between the random variables) from the population identified in subsection 3.4. For each realization, the damage trajectory is computed using the 2SD model. In the special case where the damage reaches the realization of the critical damage before t_{end}, the final damage is therefore set equal to the critical damage and the computation is stopped. This method is applied to the structure defined in Figure 8 for each of the three signals. In Figure 11, the final damage distributions $D^{\mu}(t_{end})$ are plotted for each of the signals. Regardless of the signals, the distributions have the same shape: asymmetric and defined on the same support as D_C, i.e. $[0; 0.5]$. Similarly, the expectations for the final damage are the same regardless of the load: 0.1123 ± 0.025. Thus, this distributions differ mainly in their variance and distribution tail. For example, the 8^{th} decile is 0.88 for $\sigma_1(x_0, y_0, t)$, 0.87 for $\sigma_2(x_0, y_0, t)$ and 0.80 for $\sigma_3(x_0, y_0, t)$.

Moreover, distributions of $D^{\mu}(t_{end})$ and D_C are very different. This means that D_C is not the only random variable acting on $D^{\mu}(t_{end})$. This is the reason why, the influence of the other random variables is examined by setting up $\bar{\boldsymbol{Z}}$ as the vector of material random variables that cause final damage greater than or equal to the critical damage; in other words, the vector of random variables leading to failure. In Figure 12, distributions of $\boldsymbol{Z}$ and $\bar{\boldsymbol{Z}}$ are plotted as a function of applied load. The distributions of $\boldsymbol{Z}$ are normalized, while the distributions of

$\bar{\boldsymbol{Z}}$ are plotted such that the proportionality relation between the number of failed realizations obtained and the P realizations is respected. Regardless of the load, distributions of $\bar{C}$ and C are approximately the same. On the other hand, distributions of $(\bar{S}, \bar{D}_C, \bar{p}_D)$ and (S, D_C, p_D) are very different. For low values of S and D_C almost all realizations lead to failure. This is justified by taking the equations of the 2SD model presented in subsection 2.1:

- the lower S, the higher $dD^{\mu}(t)$
- the lower D_C, the sooner the failure
- the lower p_D, the sooner the damage is initiated

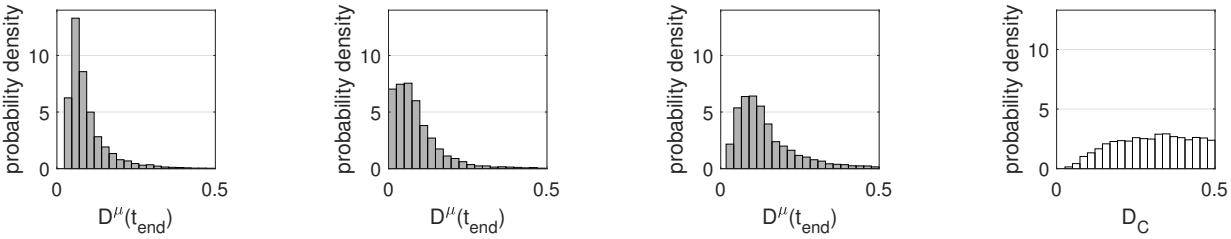

(a) First loading (b) Second loading (c) Third loading (d) For all loadings

Figure 11: Probability densities of $D^{\mu}(t_{end})$ (computed with the 2SD model) and D_C

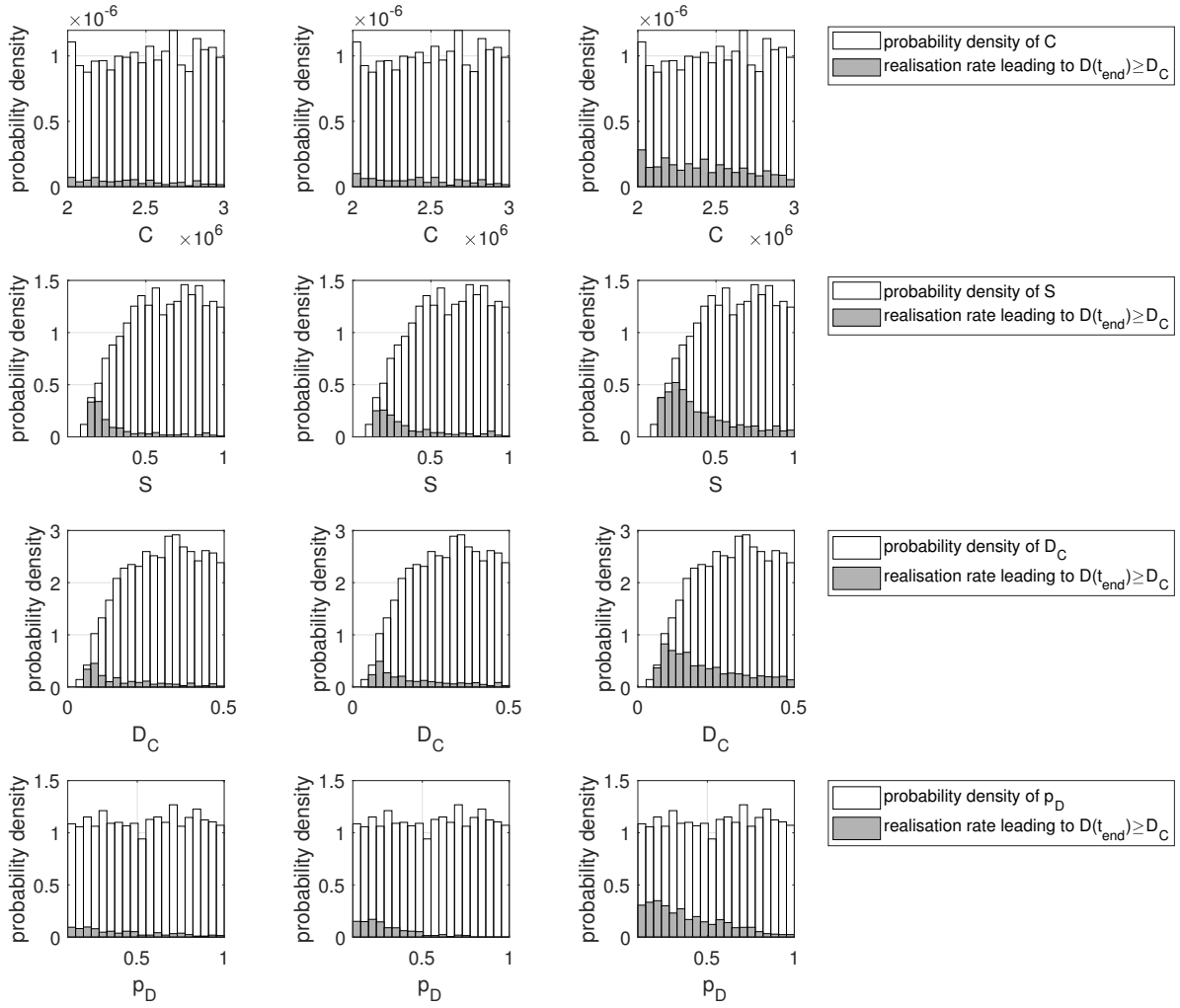

(a) First loading (b) Second loading (c) Third loading

Figure 12: Comparison of probability densities between $\boldsymbol{Z}$ and $\bar{\boldsymbol{Z}}$

4.3. Fatigue damage sensitivity analysis

To better understand how the 2SD model behaves with respect to the random variables, a sensitivity analysis of the damage is performed. Many approaches exist [45]. Three criteria have been formulated to select the most appropriate: it must be global (by taking into account the whole domain of definition of random variables), able to take into account the distribution of the parameters as well as their correlation and be robust. Since Borgonovo's method [48] meets these criteria, this method is applied with the Uqlab framework [49]. The time variant sensitivity index $\delta(D^{\mu}(t), Z_j)$ of $D^{\mu}(t)$ with respect of Z_j is then written:

$$\delta(D^{\mu}(t), Z_j) = \frac{1}{2} \int_{Z_{j_{\min}}}^{Z_{j_{\max}}} f_{Z_j}(z_j) \int_{D_{C_{\min}}}^{D_{C_{\max}}} \left| f_{D^{\mu}(t)}(D^{\mu}(t)) - f_{D^{\mu}(t)|Z_j}(D^{\mu}(t)|z_j) \right| dD^{\mu}(t) dz_j \quad (28)$$

where f_{Z_j} and $f_{D^\mu(t)}$ are the probability distribution functions of Z_j and $D^\mu(t)$, respectively. Figure 13 shows the sensitivities of the damage with respect to the random variables over time. The regularity of the trend suggests that the size of the population and the estimation technique of the indexes are suitable. These results can be explained by considering the equations of the model:

- D_C is used only when $D^\mu(t) = D_C$. As time progresses, the number of trajectories that have reached D_C increases. It is therefore consistent that $\delta(D^\mu(t), D_C)$ starts from zero and then increases with time.

- p_D is used only when the damage is initiated, i.e. $p^\mu(t) = p_D$. In a first step, as the number of trajectories reaches p_D, $\delta(D^\mu(t), p_D)$ increases with time. In a second step, the number of trajectories that reach p_D is not large enough compared to the number of trajectories that have already exceeded it and $\delta(D^\mu(t), p_D)$ starts to decrease until it reaches zero.

- C is used in the computation of the hardening:

$$D^\mu(t) = 1 - \sqrt{\frac{3}{2}} \frac{||\boldsymbol{dX^\mu}(t)||}{C dp^\mu(t)} \tag{29}$$

  By definition, $D^\mu(t)$ increases with time. Therefore, the ratio $\frac{||\boldsymbol{dX^\mu}(t)||}{dp^\mu(t)}$ decreases with time. Thus, $\delta(D^\mu(t), C)$ increases until the onset of damage and once the majority of trajectories reach p_D, the ratio $\frac{||\boldsymbol{dX^\mu}(t)||}{dp^\mu(t)}$ causes a decrease in the weight of C, making $\delta(D^\mu(t), C)$ decrease.

- S is used in the computation of the damage:

$$dD^\mu(t) = \frac{Y^\mu(t)}{S} dp^\mu(t). \tag{30}$$

  To understand the evolution of $\delta(D^\mu(t), S)$, it is necessary to study the behavior of $Y^\mu(t)dp^\mu(t)$ with time. Since (30) only allows to conclude that this term is positive, a numerical study was therefore performed. As shown Figure 14, the product $Y^\mu(t)dp^\mu(t)$ oscillates with time and that its envelope curve increases. $\delta(D^\mu(t), S)$ will increase rapidly

at first when the damage initiates. Then its speed will decrease because it is no longer due to the onset of damage, but to the term $Y^{\mu}(t)dp^{\mu}(t)$.

The evolution of the sensitivity indexes is similar regardless of the load. The main difference is the time at which the intersection between $\delta(D^{\mu}, D_C)$ and $\delta(D^{\mu}, p_D)$ occurs. In fact, for $\sigma_1(x_0, y_0, t)$ it occurs at $t_1 = 6\ 676$s, for $\sigma_3(x_0, y_0, t)$ it occurs at $t_3 = 9\ 382$s, and for $\sigma_2(x_0, y_0, t)$ it does not occur in the considered time interval. This intersection happens when the number of trajectories where $p^{\mu} = p_D$ is equal to the number of trajectories where $D^{\mu} = D_C$. Note that $t_1 \ll t_3 < t_{end}$. $\sigma_1(x_0, y_0, t)$ and $\sigma_2(x_0, y_0, t)$ were defined to cause the same final damage for the same number of cycles according to the RSN approach. Damage initiates later when the signal has a variable amplitude (compared to constant amplitude). Then $\sigma_3(x_0, y_0, t)$ was defined as equivalent to $\sigma_2(x_0, y_0, t)$ with an additional noise. Thus, for the same considered time interval, $\sigma_3(x_0, y_0, t)$ is composed of a larger number of cycles than $\sigma_2(x_0, y_0, t)$. Therefore, the damage is initiated earlier for $\sigma_3(x_0, y_0, t)$.

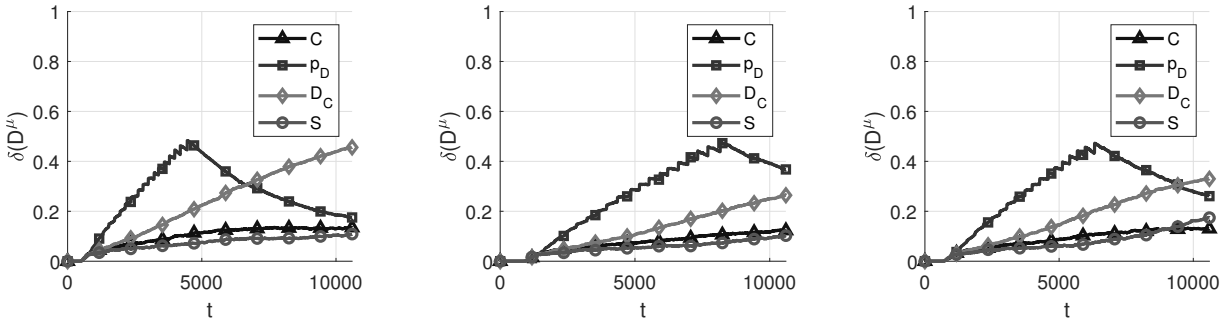

(a) First loading (b) Second loading (c) Third loading

Figure 13: Sensitivity analysis of D^{μ} with respect to $\boldsymbol{Z}$: $\delta(D^{\mu}, \boldsymbol{Z})$

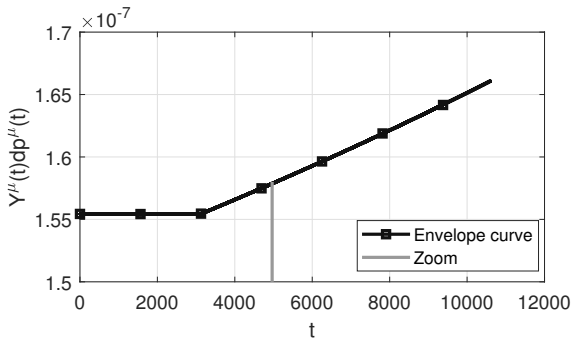

(a) Envelope curve

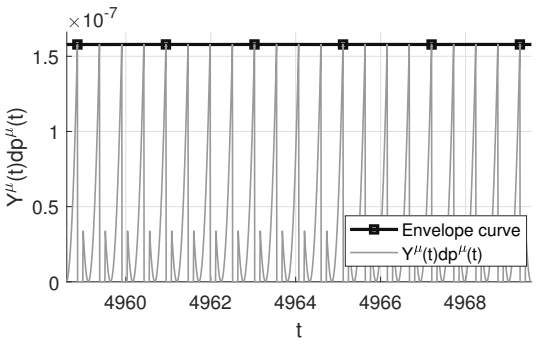

(b) Truncated evolution where $t \in [4958.6; 4969.5]$

Figure 14: First Loading, $Y^{\mu}(t)dp^{\mu}(t)$ as function of time
where $C = 2.507{\times}10^6$ MPa, $S = 0.612$ MPa, $D_C = 0.303$ and $p_D = 0.554$

To conclude, this sensitivity analysis shows that, regardless of the load, the damage is initially mostly sensitive to p_D and then to D_C.

4.4. Comparison of the probabilities of failure between the RSN approach and the 2SD model

The instantaneous probabilities of failure are defined as follows, according to the definition of the damage:

- $P_{f_q}^{RSN}(t) = \text{Prob}\left(1 - D(t) \leq 0\right)$ where the dammage is computed with (27)
- $P_{f_q}^{2SD}(t) = \text{Prob}\left(D_C - D^{\mu}(t) \leq 0\right)$ where the dammage is computed with (1) to (8)

The final probabilities of failure obtained for each of the three loads are reported in the Table 5. First, as expected, the probabilities of failure obtained with the RSN approach are equivalent for the first two loads:

$$P_{f_1}^{RSN}(t_{end}) \simeq P_{f_2}^{RSN}(t_{end}) \simeq 2.3\% \tag{31}$$

Second, the difference obtained for 2SD model and RSN approach is about 1 point. This corresponds to the error made in the calibration of the material parameters in Section 3. Third, the different results between the two methods for loads 2 and 3 illustrate the effect of loading

history on the final damage. We observed that:

$$P_{f_2}^{2SD}(t_{end}) \simeq 2P_{f_2}^{RSN}(t_{end}) \tag{32}$$

$$P_{f_3}^{2SD}(t_{end}) \simeq 3P_{f_3}^{RSN}(t_{end}) \tag{33}$$

It is clear these differences are significant and highlight the limits of a linear accumulation of damage.

	First loading	Second loading	Third loading
2SD model	166	206	662
RSN approach	109	109	263

Table 4: Number of failed realizations

	First loading	Second loading	Third loading
2SD model	3.5	4.3	13.1
RSN approach	2.3	2.3	5.5

Table 5: Probability of failure $P_{f_q}(t_{end})$ (%)

5. Conclusion and outlook

The planning of maintenance operations is a challenge. Accurate numerical tools able to quantify the state of a structure are a great help for decision making. However, to develop such objects, it is necessary to formulate as few approximations as possible. In the context of steel structures subjected to polycyclic fatigue, this is precisely the objective of the proposed work. By selecting a continuous damage model and calibrating its material parameters from random SN-curves, a method accounting for both loading history and material hazard is proposed.

First, a Bayesian calibration of the uncertain material parameters is developed and carried out in three steps: selection of uncertain parameters, choice of prior distributions and Bayesian calibration. The main contributions are the implementation of a strategy for selecting prior supports, the exploitation of variability in MCMC output and the achievement of results that guaranty conservative SN-curves. The Bayesian calibration enables to provide distributions for

the four material parameters representing material randomness where C and p_D are independent and are following a uniform law while S and D_C are correlated and are following a lognormal law.

Second, the two scale continuous damage model enables to take into account the history of damage evolution and does not require cycles counting step. This model is compared to the RSN approach using three loadings on a T-joint. For a signal with a constant stress amplitude, RSN approach and 2SD model give equivalent probability of failure. For complex signals (with random stress amplitudes), the RSN approach leads to an underestimation of the probability of failure by a factor 2 and 3. This paper thus quantifies, in a stochastic context, the interest for a non-linear damage assessment and opens its use for structural health monitoring objectives where time histories are measured.

However, the proposed method has a major drawback compared to the RSN approach: the extremely high numerical cost. Future work will therefore focus on the development of strategies to keep the numerical cost as low as possible. In particular, the implementation of a metamodel adapted to continuous damage models for time-dependent reliability will be investigated. The idea is to metamodel a control variable selected from the sensitivity analyses performed in this paper. As shown by the sensitivity analysis of damage as a function of random material variables, loading does not affect the sensitivity and thus the choice of control variable. The development of this metamodel should be a key element to account for more complex structures, a larger number of damageable elements, and geometric variability. It is mandatory for using this method inside digital twins for updating damage from monitoring.

Appendix A. Application of the 2SD model in 1D with a constant stress amplitude

A sinusoidal signal of constant amplitude $\Delta\sigma$ is considered. Figure A.15 represents the evolution of macroscopic (red) and microscopic (black) stresses during a loading cycle OABCD.

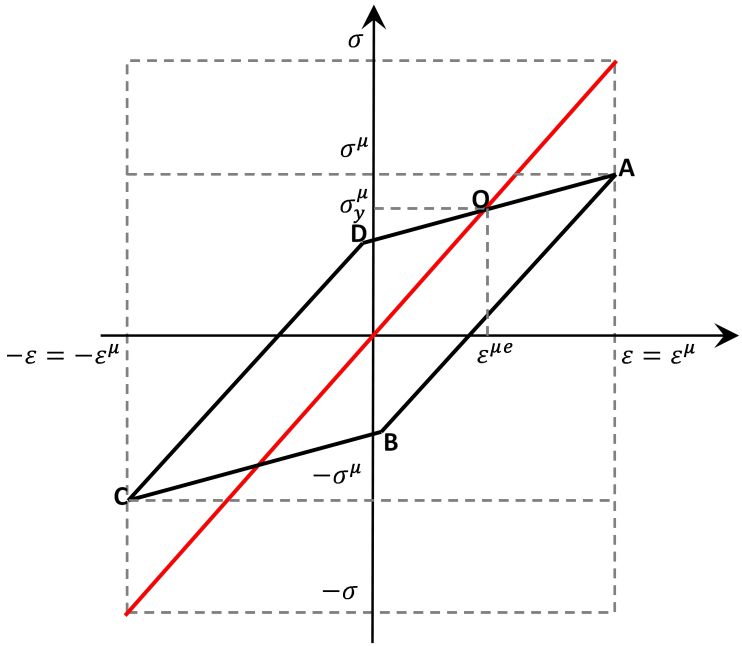

Figure A.15: Stress-strain diagram of the 2SD model during a loading cycle OABCD, [26]

Before damage initiation, with $\varepsilon = \varepsilon^\mu$ and $\varepsilon^\mu = \varepsilon^{\mu e} + \varepsilon^{\mu p}$, the microscopic plastic strain writes:

$$\varepsilon^{\mu p} = \varepsilon - \varepsilon^{\mu e} \tag{A.1}$$

With Hooke's law $E\varepsilon = \sigma$ at the macroscopic scale and $E\varepsilon^{\mu e} = \tilde{\sigma}^\mu$ at the microscopic, the previous expression becomes:

$$E\varepsilon^{\mu p} = \sigma - \tilde{\sigma}^\mu \tag{A.2}$$

In addition, during the OA transformation $\tilde{\sigma}^\mu - X^\mu > 0$, the yield surface where is written:

$$f = |\tilde{\sigma}^\mu - X^\mu| - \sigma_y^\mu = 0 \Rightarrow X^\mu = \tilde{\sigma}^\mu - \sigma_y^\mu \tag{A.3}$$

Because the initial damage is 0, $\tilde{\sigma}^\mu = \sigma^\mu$ so the previous expression becomes:

$$X^\mu = \sigma^\mu - \sigma_y^\mu \tag{A.4}$$

From the linear kinematic hardening formulation and (A.4), the microscopic plastic strain is

expressed such that:

$$dX^{\mu} = \frac{2}{3} C d\varepsilon^{\mu p} \Rightarrow \varepsilon^{\mu p} = \frac{3}{2C}(\sigma^{\mu} - \sigma_y^{\mu}) \tag{A.5}$$

Thus, with (A.2) and (A.5), the microscopic stress writes:

$$\sigma^{\mu} = \frac{2C\sigma + 3E\sigma_y^{\mu}}{2C + 3E} \tag{A.6}$$

And with (A.4) and (A.6), the linear kinematic hardening reads:

$$X^{\mu} = \frac{2C(\sigma - \sigma_y^{\mu})}{2C + 3E} \tag{A.7}$$

Moreover since a cycle corresponds to a microscopic plastic accumulation $\Delta p^{\mu} = 4\varepsilon^{\mu p}$, with (A.5) the previous equation becomes:

$$\Delta p^{\mu} = \frac{12(\sigma - \sigma_y^{\mu})}{2C + 3E} \tag{A.8}$$

Finally, the number of cycles N_D necessary to initiate the damage is:

$$N_D \Delta p^{\mu} = p_D \tag{A.9}$$

$$N_D = \frac{2C + 3E}{12(\sigma - \sigma_y^{\mu})} p_D \tag{A.10}$$

According to the definition of the release rate of elastic energy and Hook's law, Y^{μ} is written:

$$Y^{\mu} = \frac{1}{2} \tilde{\sigma}^{\mu} \varepsilon^{\mu e} \tag{A.11}$$

$$Y^{\mu} = \frac{\tilde{\sigma}^{\mu^2}}{2E} \tag{A.12}$$

With (A.3), the increment of hardening is formulated $dX^{\mu} = d\tilde{\sigma}^{\mu}$. Thus, according to the equation (A.5), the increment of microscopic plastic strain is expressed:

$$d\varepsilon^{\mu p} = \frac{3}{2C} d\tilde{\sigma}^{\mu} \tag{A.13}$$

From the definition of the damage and the two previous equations, the damage increment is written:

$$dD^{\mu} = \left(\frac{Y^{\mu}}{S}\right)^{s} dp^{\mu} \tag{A.14}$$

$$dD^{\mu} = \left(\frac{\tilde{\sigma}^{\mu^2}}{2ES}\right)^{s} \frac{3}{2C} |d\tilde{\sigma}^{\mu}| \tag{A.15}$$

The damage associated to one cycle is :

$$\Delta D^{\mu} = \int_{OABCD} dD^{\mu} \tag{A.16}$$

$$\Delta D^{\mu} = \frac{3}{2C(2ES)^{s}} \int_{OABCD} \tilde{\sigma}^{\mu^{2s}} |d\tilde{\sigma}^{\mu}| \tag{A.17}$$

$$\Delta D^{\mu} = \frac{3}{C(2ES)^{s}} \int_{DOA} \tilde{\sigma}^{\mu^{2s}} d\tilde{\sigma}^{\mu} \tag{A.18}$$

Since in A, $\tilde{\sigma}_A^{\mu} = \tilde{\sigma}^{\mu}$ and in D, $\tilde{\sigma}_A^{\mu} = \sigma_y^{\mu} - (\tilde{\sigma}_A^{\mu} - \sigma_y^{\mu}) = 2\sigma_y^{\mu} - \tilde{\sigma}^{\mu}$ then the bounds of the integrals are written:

$$\Delta D^{\mu} = \frac{3}{C(2ES)^{s}} \int_{2\sigma_y^{\mu} - \tilde{\sigma}^{\mu}}^{\tilde{\sigma}^{\mu}} \tilde{\sigma}^{\mu^{2s}} d\tilde{\sigma}^{\mu} \tag{A.19}$$

$$\Delta D^{\mu} = \frac{3\left(\tilde{\sigma}^{\mu^{2s+1}} - (2\sigma_y^{\mu} - \tilde{\sigma}^{\mu})^{2s+1}\right)}{C(2ES)^{s}(2s+1)} \tag{A.20}$$

Since $dN\Delta D^{\mu} = dD^{\mu}$, the formulation of the number of cycles to failure is:

$$dN = \frac{C(2ES)^{s}(2s+1)}{3\left(\tilde{\sigma}^{\mu^{2s+1}} - (2\sigma_y^{\mu} - \tilde{\sigma}^{\mu})^{2s+1}\right)} dD^{\mu} \tag{A.21}$$

$$\int_{N_D}^{N} dN = \frac{C(2ES)^{s}(2s+1)}{3\left(\tilde{\sigma}^{\mu^{2s+1}} - (2\sigma_y^{\mu} - \tilde{\sigma}^{\mu})^{2s+1}\right)} \int_{0}^{D_C} dD^{\mu} \tag{A.22}$$

$$N = N_D + \frac{C(2ES)^{s}(2s+1)}{3\left(\tilde{\sigma}^{\mu^{2s+1}} - (2\sigma_y^{\mu} - \tilde{\sigma}^{\mu})^{2s+1}\right)} D_C \tag{A.23}$$

Finally, with (A.10) and knowing that $\Delta\sigma = 2\sigma$, the previous equation becomes :

$$N = \frac{2C + 3E}{6(\Delta\sigma - 2\sigma_y^{\mu})} p_D + \frac{C(2ES)^{s}(2s+1)}{3\left(\tilde{\sigma}^{\mu^{2s+1}} - (2\sigma_y^{\mu} - \tilde{\sigma}^{\mu})^{2s+1}\right)} D_C \tag{A.24}$$

Appendix B. Application of the 2SD model to illustrate the ability of the model to take into account the loading history

The effect of the loading history is illustrated by comparing the 2SD model with the RSN approach. Two stress signals $\sigma_{SL}(t)$ and $\sigma_{LS}(t)$ are defined from $\sigma_1(t)$. They are both composed of $n^* = 10^4$ cycles.

- $\sigma_{SL}(t)$ is composed of a sinusoidal signal of amplitude $\Delta\sigma_S = 0.5\Delta\sigma_{1,1} = 192.5$ MPa on $[0; \frac{2}{3}t_{end}]$ and a sinusoidal signal of amplitude $\Delta\sigma_L = 1.25\Delta\sigma_{1,1} = 481.25$ MPa on $[\frac{2}{3}t_{end}; t_{end}]$.
- $\sigma_{LS}(t)$ is composed of a sinusoidal signal of amplitude $\Delta\sigma_L = 1.25\Delta\sigma_{1,1} = 481.25$ MPa on $[0; \frac{1}{3}t_{end}]$ and a sinusoidal signal of amplitude $\Delta\sigma_S = 0.5\Delta\sigma_{1,1} = 192.5$ MPa on $[\frac{1}{3}t_{end}; t_{end}]$.

First, the damage analysis is done for one deterministic material of parameters $C = 2.5 \times 10^6$ MPa, $D_C = 0.25$, $p_D = 0.5$ and $S = 0.5$ MPa. The two signals lead to the same final damage with the RSN approach. On Figure B.16, the evolution of damage computed with the 2SD model is given. It is clearly observed that the final damage is not the same for the two signals.

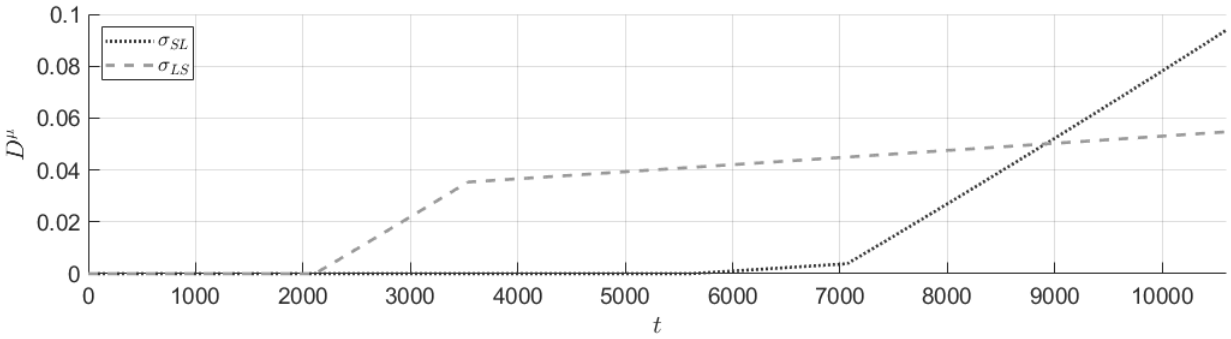

Figure B.16: Damage trajectories computed with the 2SD model for $\sigma_{SL}(t)$ and $\sigma_{LS}(t)$

Second, a probabilistic study is performed. As in subsection 4.2, the material uncertainties are propagated by considering a sample P of 5000 realizations. Four probabilities of failure are computed and plotted in Figure B.17:

- $P_{f_{SL}}^{RSN}(t)$ where the damage is computed with the RSN approach by considering $\sigma_{SL}(t)$
- $P_{f_{LS}}^{RSN}(t)$ where the damage is computed with the RSN approach by considering $\sigma_{LS}(t)$
- $P_{f_{SL}}^{2SD}(t)$ where the damage is computed with the 2SD model by considering $\sigma_{SL}(t)$

- $P_{f_{LS}}^{2SD}(t)$ where the damage is computed with the 2SD model by considering $\sigma_{LS}(t)$

At $t = t_{end}$, with the RSN approach, the probabilities of failure are equal:

$$P_{f_{SL}}^{RSN}(t_{end}) = P_{f_{LS}}^{RSN}(t_{end}) \tag{B.1}$$

However, the 2SD model takes into account the loading history and the probabilities of failure are clearly distinct:

$$P_{f_{SL}}^{2SD}(t_{end}) \simeq 4P_{f_{LS}}^{2SD}(t_{end}) \tag{B.2}$$

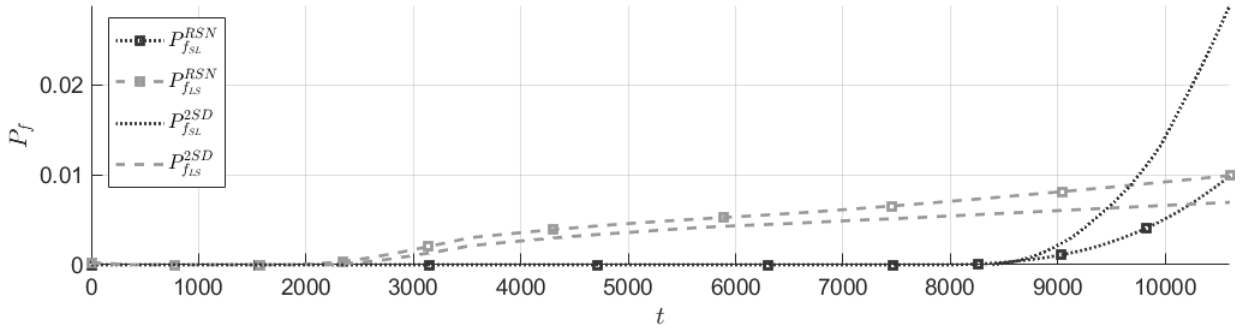

Figure B.17: Probabilities of failure for $\sigma_{SL}(t)$ and $\sigma_{LS}(t)$

References

[1] M. Faber and J. Sorensen, "Indicators for inspection and maintenance planning of concrete structures," *Structural Safety*, vol. 24, no. 2, pp. 377–396, 2002.

[2] A. Rouhan and F. Schoefs, "Probabilistic modeling of inspection results for offshore structures," *Structural Safety*, vol. 25, pp. 379–399, 2003.

[3] H. Queiroz, J. Araújo, C. Silva, and J. Ferreira, "A coupled critical plane-area methodology to estimate fatigue life for an aisi 1045 steel with small artificial defects," *Theoretical and Applied Fracture Mechanics*, vol. 121, p. 103426, 2022.

[4] A. Cruces, A. Garcia-Gonzalez, B. Moreno, T. Itoh, and P. Lopez-Crespo, "Critical plane based method for multiaxial fatigue analysis of 316 stainless steel," *Theoretical and Applied Fracture Mechanics*, vol. 118, p. 103273, 2022.

[5] H. Mahmoud and G. Riveros, "Fatigue reliability of a single stiffened ship hull panel," *Engineering Structures*, vol. 66, pp. 89–99, 2014.

[6] I. Gledić, J. Parunov, P. Prebeg, and M. Ćorak, "Low-cycle fatigue of ship hull damaged in collision," *Engineering Failure Analysis*, vol. 96, pp. 436–454, 2019.

[7] Y. Dong, Y. Garbatov, and C. Guedes Soares, "Strain-based fatigue reliability assessment of welded joints in ship structures," *Marine Structures*, vol. 75, p. 102878, 2021.

[8] C. Han, C. Mo, L. Tao, Y. Ma, and X. Bai, "An efficient fatigue assessment model of offshore wind turbine using a half coupling analysis," *Ocean Engineering*, vol. 263, p. 112318, 2022.

[9] D. Haselibozchaloee, J. Correia, P. Mendes, A. de Jesus, and F. Berto, "A review of fatigue damage assessment in offshore wind turbine support structure," *International Journal of Fatigue*, vol. 164, p. 107145, 2022.

[10] O. Pasqualini, F. Schoefs, M. Chevreuil, and M. Cazuguel, "Measurements and statistical analysis of fillet weld geometrical parameters for probabilistic modelling of the fatigue capacity," *Marine Structures*, vol. 34, pp. 226–248, 2013.

[11] F. Schoefs, M. Chevreuil, O. Pasqualini, and M. Cazuguel, "Partial safety factor calibration from stochastic finite element computation of welded joint with random geometries," *Reliability Engineering & System Safety*, vol. 155, pp. 44–54, 2016.

[12] W. Du, S. Li, and Y. Luo, "A novel method for structure's fatigue life scatter simulation under material variability," *International Journal of Fatigue*, vol. 149, p. 106296, 2021.

[13] V. Giannella, R. Sepe, and R. Citarella, "Fatigue crack propagation for an aircraft compressor under input data variability," *Procedia Structural Integrity*, vol. 41, pp. 298–304, 2022. 2nd Mediterranean Conference on Fracture and Structural Integrity.

[14] J. Velarde, C. Kramhøft, and J. D. Sørensen, "Global sensitivity analysis of offshore wind turbine foundation fatigue loads," *Renewable Energy*, 2019.

[15] H. Ameryoun, F. Schoefs, L. Barillé, and Y. Thomas, "Stochastic modeling of forces on jacket-type offshore structures colonized by marine growth," *Journal of Marine Science and Engineering*, 2019.

[16] F. Schoefs, "Sensitivity approach for modelling the environmental loading of marine structures through a matrix response surface," *Reliability Engineering & System Safety*, vol. 93, no. 7, pp. 1004–1017, 2008. Bayesian Networks in Dependability.

[17] A. Fatemi and L. Yang, "Cumulative fatigue damage and life prediction theories: a survey of the state of the art for homogeneous materials," *International Journal of Fatigue*, vol. 20, no. 1, pp. 9–34, 1998.

[18] DNV, "Rp-c203: Fatigue of offshore steel structures," 2014.

[19] N. Hong, "A modified rainflow counting method," *International Journal of Fatigue*, vol. 13, no. 6, pp. 465–469, 1991.

[20] A. Palmgren, "Die lebensdauer von kugellargern," 1924.

[21] M. A. Miner, "Cumulative damage in fatigue," *Journal of Applied Mechanics*, vol. 12, pp. A159–A164, 03 2021.

[22] J. Lemaître, "A course on damage mechanics," 1992.

[23] G. A. Francfort and J.-J. Marigo, "Stable damage evolution in a brittle continuous medium," *European Journal of Mechanics A-solids*, vol. 12, pp. 149–189, 1993.

[24] O. Allix, P. Ladevèze, D. Gilletta, and R. Ohayon, "A damage prediction method for composite structures," *International Journal for Numerical Methods in Engineering*, vol. 27, pp. 271–283, 1989.

[25] J. Lemaitre and I. Doghri, "Damage 90: a post processor for crack initiation," *Computer Methods in Applied Mechanics and Engineering*, vol. 115, no. 3, pp. 197–232, 1994.

[26] B. Rocher, F. Schoefs, M. François, A. Salou, and A.-L. Caouissin, "A two-scale probabilistic time-dependent fatigue model for offshore steel wind turbines," *International Journal of Fatigue*, vol. 136, p. 105620, 2020.

[27] A. Banvillet, T. Palin-Luc, and S. Lasserre, "A volumetric energy based high cycle multiaxial fatigue citerion," *International journal of fatigue*, vol. 25, no. 8, pp. 755–769, 2003.

[28] K. VAN and B. Griveau, "On a new multiaxial fatigue limit criterion- theory and application," *Biaxial and multiaxial fatigue(A 90-16739 05-39). London, Mechanical Engineering Publications, Ltd., 1989,*, pp. 479–496, 1989.

[29] C.-M. Suh and H. Kitagawa, "Crack growth behaviour of fatigue microcracks in low carbon steels," *Fatigue & Fracture of Engineering Materials & Structures*, vol. 9, pp. 409–424, 1987.

[30] M. Zhang, P. Yang, Y. Tan, Y. Liu, and S. Gong, "An observation of crack initiation and early crack growth under impact fatigue loading," *Materials Science and Engineering A-structural Materials Properties Microstructure and Processing*, vol. 271, pp. 390–394, 1999.

[31] J. Lemaitre and J.-L. Chaboche, "Aspect phénoménologique de la rupture par endommagement," *J Méc Appl*, vol. 2, no. 3, 1978.

[32] J. Lemaître and R. Desmorat, "Engineering damage mechanics: Ductile, creep, fatigue and brittle failures," 2005.

[33] R. Desmorat and J. Lemaître, "Section 6.15 – a two-scale model for quasi-brittle and fatigue damage," 2001.

[34] A. de Recherche sur les Structures Métalliques Marines, *Assemblages tubulaires soudés. Guides Pratiques sur les Ouvrages en Mer.* Technip, Paris, 1985.

[35] W. L. Oberkampf, T. G. Trucano, and C. Hirsch, "Verification, validation, and predictive capability in computational engineering and physics," *Applied Mechanics Reviews*, vol. 57, pp. 345–384, 2004.

[36] W. L. Oberkampf and C. J. Roy, *Verification and Validation in Scientific Computing.* Cambridge University Press, 2010.

[37] K. T. Hu and G. E. Orient, "The 2014 Sandia Verification and Validation Challenge: Problem Statement," *Journal of Verification, Validation and Uncertainty Quantification*, vol. 1, 02 2016. 011001.

[38] G. Jiao and T. Moan, "Methods of reliability model updating through additional events," *Structural Safety*, vol. 9, no. 2, pp. 139–153, 1990.

[39] C. W. Fox and S. J. Roberts, *A tutorial on variational Bayesian inference.* Artificial Intelligence Review, 2012.

[40] Y. M. Marzouk, T. Moselhy, M. D. Parno, and A. Spantini, "An introduction to sampling via measure transport," *arXiv: Computation*, 2016.

[41] C. P. Robert and G. Casella, "Monte carlo statistical methods," *Technometrics*, vol. 47, pp. 243 – 243, 2005.

[42] N. Metropolis, A. W. Rosenbluth, M. N. Rosenbluth, A. H. Teller, and E. Teller, "Equation of state calculations by fast computing machines," *Journal of Chemical Physics*, vol. 21, pp. 1087–1092, 1953.

[43] W. K. Hastings, "Monte carlo sampling methods using markov chains and their applications," *Biometrika*, vol. 57, pp. 97–109, 1970.

[44] J. Lemaître, "Handbook of materials behavior models," 2001.

[45] F. Pianosi, K. J. Beven, J. E. Freer, J. W. Hall, J. Rougier, D. B. Stephenson, and T. Wagener, "Sensitivity analysis of environmental models: A systematic review with practical workflow," *Environ. Model. Softw.*, vol. 79, pp. 214–232, 2014.

[46] M. Moustapha, N. Fajraoui, S. Marelli, and B. Sudret, "Uqlab user manual – random fields, chair of risk, safety and uncertainty quantification," 2022.

[47] R. G. Ghanem and P. D. Spanos, "Spectral stochastic finite-element formulation for reliability analysis," *Journal of Engineering Mechanics-asce*, vol. 117, pp. 2351–2372, 1991.

[48] E. Borgonovo, "A new uncertainty importance measure," *Reliability Engineering & System Safety*, vol. 92, no. 6, pp. 771–784, 2007.

[49] S. Marelli, C. Lamas, K. Konakli, C. Mylonas, P. Wiederkehr, and B. Sudret, "Uqlab user manual – sensitivity analysis, chair of risk safety and uncertainty quantification," 2022.